by anti-inflammatory cytokines, such as IL-4, IL-13, and IL-10, to ameliorate type 1 inflammatory responses and control adaptive immunity. Furthermore, their anti-inflammatory cytokines promote and regulate type 2 immune responses, angiogenesis, and tissue repair.[41]

In this regard, monocyte/macrophages in QQMNCs mainly adopt angiogenic and anti-inflammatory phenotypes and are contributing to regenerative process in ischemic organs.

Among lymphocyte lineage cells, B lymphocytes, NK cells, and cytotoxic T cells significantly decrease or fade away. Instead, helper T cells are the last surviving lymphocyte population in QQ cultures. The phenotype identification of $CD4^+$ cells disclosed the significant increase in $CD4^+$/$CD25^+$/$Foxp3^+$ regulatory T lymphocytes as well as $CD4^+$/$IL\text{-}4^+$ Th2 lymphocytes. In recent years, the interaction between monocytes/macrophages and T lymphocytes has been investigated. IFN-γ produced by Th1 lymphocytes induce monocytes to become classical activated M1 macrophages, whereas IL-4, IL-13, and IL-10 that are produced by Th2 and regulatory T lymphocytes induce differentiation of regenerative M2 macrophages. IL-12 and IL-6 produced by M1 macrophages activate Th1 lymphocytes, whereas IL-10 and TGF-β produced by M2 macrophages encourage Th2 and regulatory T-lymphocyte functions.[41,42]

Therefore, the cell-cell interactions among M2 macrophages, Th2, and regulatory T cells are considered to accelerate QQMNCs function as angiogenic and anti-inflammatory tools.

Of note, the majority of T lymphocytes in QQ cultures are $CXCR4^+$/$CD31^+$/$CD3^+$ cells. This population is called "angiogenic T cells" in the vascular biology field; these T cells deliver proangiogenic cytokines in tissues for neovascularization.[30] The finding also encourages that the phenotype of T lymphocytes is conducible to angiogenic preference of QQMNCs.

Therefore, QQMNCs signal regenerative switches on PBMNCs not only by EPC expansion and differentiation, but also through collaborative M2 macrophage polarization and Th2 and regulatory T-cell activation in QQ culture.

Cross-Talk of Cell Populations in QQMNCs

The finding shown in Figure 1F indicates that $CD34^+$ cell-depleted PBMNCs included some cell population to accelerate EPC expansion and differentiation in $CD34^+$ cells through QQ culture. As demonstrated in Figure 2C and 2D, EPCs, M2 macrophage, Th2, and regulatory T lymphocytes were mainly activated in QQMNCs. Increasingly, researches are focused on the interaction between macrophages and T lymphocytes to elucidate the collaborative mechanism of inflammation and immunity. Although we do not have any evidence to indicate that EPCs are involved in this collaboration, the developed culture for EPC expansion, QQ culture, regulates phenotypes of macrophages and T lymphocytes and, consequently, exerts EPC expansion and differentiation. Therefore, any cellular or molecular mechanism responsible for the effects of $CD34^+$ cell-depleted PBMNCs needs to be identified in the future for scientific and therapeutic interests.

Factors Expressed From QQMNCs

In order to further examine the vasculogenic potential of QQMNCs, qRT-PCR was used to determine gene expression profiles. In QQMNCs, the expression of mRNAs encoding anti-inflammatory and proangiogenic factors was enhanced, whereas that of mRNAs encoding proinflammatory cytokines declined (Figure 3).

Expression of mRNAs encoding proangiogenic cytokines and growth factors (eg, IL-10,[43] leptin,[44,45] IGF-1,[46] and IL-8[47]) was greatly elevated. Leptin[45] and IL-10[48] promote the vasculogenic and angiogenic potentials of EPCs and ECs. IGF-1[49] and IL-8[50] are also related factors responsible for angiogenic properties of EPCs. Furthermore, IGF-1 promotes muscle fiber regeneration[35]; this phenomenon may be reflected in the findings of enhanced myogenesis after QQMNCTx. VEGF-B and Angn-1 were up-regulated in QQMNCs, and they potentiate vascular survival and maturation relating to arteriogenesis induced by pericyte recruitment.[33,34] However, expression of mRNA encoding VEGF-A, one of the main proangiogenic growth factors, was not elevated, but rather reduced in QQMNCs, relative to PBMNCs. The reduction of VEGF-A expression might be explained by a negative feedback mechanism through high dose of VEGF-A protein in QQ culture conditioning.

In contrast, expression of mRNA encoding TGF-β, one of the potent anti-inflammatory factors, was lower in QQMNCs. However, expression of mRNAs encoding TNF-α and IL-1β, the important proinflammatory mediators, was similarly mitigated between QQMNCs and PBMNCs for TNF-α while prominently down-regulated in QQMNCs and in PBMNCs for IL-1β.

The findings indicate that QQMNCs may not, at least, bring proinflammatory cell populations more than PBMNCs.

Moreover, the expression of mRNAs encoding MMP-2 or -9, which, playing a critical role in neovascularization and tissue remodeling for antifibrosis,[36] were highly up-regulated.

Taken together, QQMNCTx, compared to PBMNCTx, resulted in more favorable conditions for vascular regeneration or tissue repair because of the orchestration of dynamic expression of multiple cytokines and growth factors.

Therapeutic Potential of QQMNCs for Hindlimb Ischemia Models

QQMNCs have therapeutic potential because transplantation of the cells into ischemic hindlimb tissue was associated with

increased blood flow, limb survival, and neovascularization in tissues (Figure 5). Moreover, histological findings indicate that transplanted human QQMNCs contributed to new microvessel formation composed of human cells derived from EPCs in QQMNCs, as well as mouse microvessel formation and arteriogenesis supported by pericytes (Figures 6 and 7). The latter effects were presumably the result of angiogenic paracrine effects by accelerated phenotypes of macrophages and T lymphocytes as well as EPCs.

The other categorical finding of this transplantation treatment was decreased fibrosis and inflammation as well as enhanced myogenesis (Figures 8 through 10). As indicated by cell population study and gene expression analyses, QQMNCs included many anti-inflammatory M2 macrophages; the cells had enhanced expression of the anti-inflammatory cytokine, IL-10, and the anti-fibrotic proteases, MMP-2 and -9, as well as decreased expression of the proinflammatory cytokine, IL-1β. This anti-inflammatory effect by QQMNCs conceivably protected against fibrosis, even in severe ischemic muscles. Moreover, skeletal myogenesis was also augmented by transplantation of QQMNCs with enhanced expression of mRNA encoding IGF-1.

Thus, we demonstrated that transplanted QQMNCs per se provide the favorable microenvironment for injured tissue regeneration by exerting vascularization as well as anti-inflammatory and myogenic effects.

As recently reported,[7] autologous PBMNCs isolated by apheresis and then transplanted into patients had vascular therapeutic potential, when the largest cell dose (over 1×10^{10} cells of human subject) was implanted. Here, we transplanted only 1×10^{4} cells (PBMNCs and/or QQMNCs) per mouse subject; this dose corresponds to $\approx$2.0 to 2.5×10^{7} cells in a human subject of 50 kg body weight. We implanted far fewer cells than are generally used for clinical treatments. Therefore, the effect of PBMNCs on ischemic hindlimbs was minimal, whereas QQMNCTx had extensive therapeutic effects on vascular regeneration and tissue repair.

On the other hand, the cell dose of 1×10^{4} cells per mouse subject also corresponds to that used at transplantation of G-CSF-mobilized $CD34^{+}$ cells in patients with critical limb ischemia.[17,19] Of note, in the present study, QQMNCTx exerted the experimental efficacy equal to or in part greater than that of GmCD34Tx.

The count of transplanted QQMNCs (1×10^{4} cells/mouse) for therapeutic activity of tissue regeneration corresponds to cell quantity, on average, acquired from <100 mL of PB of human subjects. The isolation and preparation of QQMNCs require only the MNC isolation and a week culture in QQ culture conditions that included recombinant factors without any manipulation. Furthermore, the process avoids invasive procedures for isolation, such as BM cell isolation or leukapheresis, and expensive costs for mobilization and target cell isolation, such as G-CSF administration or $CD34^{+}/CD133^{+}$ cell isolation using magnetic beads.

Collectively, the QQMNC is expected to be an advantageous and feasible cell source for cell-based therapy targeting ischemic diseases.

Responsive Mechanism in Ischemic Hindlimb for Tissue Regeneration After QQMNCTx

Histochemistry (Figures 8 through 10) and qRT-PCR assay (Figure 11) demonstrated that QQMNCTx, as well as GmCD34Tx, provides the preferential environment for tissue regeneration of myogenesis, antifibrosis, and anti-inflammation in the ischemic hindlimb.

With respect to qRT-PCR assay, IL-1β, a proinflammatory cytokine, has been reported to function as a proangiogenic factor derived from regenerating myoblasts responding to PBMNC implantation in the ischemic hindlimb.[51] In the present study, implantation of PBMNCs highly induced the expression of mRNA encoding IL-1β in ischemic tissue, similarly to that of QQMNCs, whereas it did not demonstrate great angiogenic potential. The causes of the dissimilar response might be presumably attributed to the distinct animal experiments using different murine strains with various cell doses for transplantation: immunodeficient BALB/c nu/nu nude mice (1×10^{4} cells/mouse) in our study and C57BL/6 mice (1×10^{6} cells/mouse) elsewhere.[51]

Notably, QQMNCTx, similarly to GmCD34Tx, up-regulated the gene expression of mRNAs encoding promyogenic factors of IGF-1,[52] MyoD1, and myogenin in the ischemic hindlimb; Tx of those cell types induced preferential myogenesis, unlike Tx of the other cell candidates, in histological evaluation.

This means that the effective myogenesis by cell transplantation may primarily require in situ IGF-1 production, which also signifies a myogenic biomarker in the ischemic hindlimb. Regarding the results, skeletal muscle-restricted expression of IGF-1 in transgenic mice has been reported to not only accelerate muscle regeneration, but also to exert the protective effects against inflammation and fibrosis in the injured skeletal muscle.[53] Moreover, IGF-1 has been reported to inhibit nuclear factor kappa B activation through TNF-α[54] or proapoptotic miRNA expression[55] in ischemic cardiomyocytes. Therefore, IGF-1 supplied to ischemic tissue by local QQMNCTx is adequately conceived to exert the protective effect on inflammation, fibrosis, or tissue injury. Also, QQMNCs per se exhibited enhanced expression of mRNA encoding human IGF-1 (Figure 3A).

Likewise, QQMNCTx, as well as GmCD34Tx, up-regulated expression of mRNA encoding TGF-β, a potent inhibitory factor of inflammation, in transplanted tissue, although

QQMNC in vitro exhibited lesser expression than PBMNCs. Unlike the aspect of IGF-1, the responsive tissue expression in situ of TGF-β after cell transplantations, might contribute to protecting against inflammation, rather than the expression by the transplanted cells.

Take together, expression of IGF-1 or TGF-β by injured tissue responsive to QQMNCTx, as well as that of IGF-1 and other tissue regeneration mediators by the transplanted cells per se, are expected to reveal the mechanism underlying the preferential efficacy of cell Tx.

Limitation of the Present Study

In the present study, recipients' T-lymphocyte-deficient condition in athymic BALB/c nu/nu nude mice limits the insight into regeneration mechanism by regulatory effects on host immune response through regulatory T cells increased in QQMNCs. Therefore, the relevant animal model studies are required to elucidate the essential effect of QQMNCTx in future experiments.

Conclusion

The QQ culture system for whole PBMNCs that we described here may lead to an effective cell-based therapy to alleviate the physical burdens in patients as one feasible strategy for vascular regeneration or tissue repair.

Acknowledgments

The authors thank the staves of Teaching and Research Support Core Center of Tokai University School of Medicine for outstanding technical support as well as Sachie Ota for her secretarial assistance.

Sources of Funding

This work was supported by grants from the Riken Center for Developmental Biology Collaborative Research Fund, Kobe (08001475), Japan, the Ministry of Health, Labor and Welfare (25280401), Japan, and the Ministry of Education, Culture, Sports, Science and Technology (Academic Frontier Promotion Program), Japan. H.M. is personally supported by the Ministry of Education, Culture, Sports, Science and Technology (Basic Research Grant No. 25461091), Japan, Tokai University School of Medicine Research Aid, and Research and Study Project of Tokai University Education System General Research Organization, Japan.

Disclosures

None.

References

1. Asahara T, Murohara T, Sullivan A, Silver M, van der Zee R, Li T, Witzenbichler B, Schatteman G, Isner JM. Isolation of putative progenitor endothelial cells for angiogenesis. *Science*. 1997;275:964–967.
2. Shi Q, Rafii S, Wu MH, Wijelath ES, Yu C, Ishida A, Fujita Y, Kothari S, Mohle R, Sauvage LR, Moore MA, Storb RF, Hammond WP. Evidence for circulating bone marrow-derived endothelial cells. *Blood*. 1998;92:362–367.
3. Asahara T, Masuda H, Takahashi T, Kalka C, Pastore C, Silver M, Kearne M, Magner M, Isner JM. Bone marrow origin of endothelial progenitor cells responsible for postnatal vasculogenesis in physiological and pathological neovascularization. *Circ Res*. 1999;85:221–228.
4. Tateishi-Yuyama E, Matsubara H, Murohara T, Ikeda U, Shintani S, Masaki H, Amano K, Kishimoto Y, Yoshimoto K, Akashi H, Shimada K, Iwasaka T, Imaizumi T; Therapeutic Angiogenesis using Cell Transplantation Study I. Therapeutic angiogenesis for patients with limb ischaemia by autologous transplantation of bone-marrow cells: a pilot study and a randomised controlled trial. *Lancet*. 2002;360:427–435.
5. Assmus B, Schachinger V, Teupe C, Britten M, Lehmann R, Dobert N, Grunwald F, Aicher A, Urbich C, Martin H, Hoelzer D, Dimmeler S, Zeiher AM. Transplantation of progenitor cells and regeneration enhancement in acute myocardial infarction (TOPCARE-AMI). *Circulation*. 2002;106:3009–3017.
6. Schachinger V, Tonn T, Dimmeler S, Zeiher AM. Bone-marrow-derived progenitor cell therapy in need of proof of concept: design of the REPAIR-AMI trial. *Nat Clin Pract Cardiovasc Med*. 2006;3(suppl 1):S23–S28.
7. Moriya J, Minamino T, Tateno K, Shimizu N, Kuwabara Y, Sato Y, Saito Y, Komuro I. Long-term outcome of therapeutic neovascularization using peripheral blood mononuclear cells for limb ischemia. *Circ Cardiovasc Interv*. 2009;2:245–254.
8. Yoon YS, Park JS, Tkebuchava T, Luedeman C, Losordo DW. Unexpected severe calcification after transplantation of bone marrow cells in acute myocardial infarction. *Circulation*. 2004;109:3154–3157.
9. Lunde K, Solheim S, Aakhus S, Arnesen H, Abdelnoor M, Egeland T, Endresen K, Ilebekk A, Mangschau A, Fjeld JG, Smith HJ, Taraldsrud E, Grogaard HK, Bjornerheim R, Brekke M, Muller C, Hopp E, Ragnarsson A, Brinchmann JE, Forfang K. Intracoronary injection of mononuclear bone marrow cells in acute myocardial infarction. *N Engl J Med*. 2006;355:1199–1209.
10. Miyamoto K, Nishigami K, Nagaya N, Akutsu K, Chiku M, Kamei M, Soma T, Miyata S, Higashi M, Tanaka R, Nakatani T, Nonogi H, Takeshita S. Unblinded pilot study of autologous transplantation of bone marrow mononuclear cells in patients with thromboangiitis obliterans. *Circulation*. 2006;114:2679–2684.
11. Moazzami K, Majdzadeh R, Nedjat S. Local intramuscular transplantation of autologous mononuclear cells for critical lower limb ischaemia. *Cochrane Database Syst Rev*. 2011;12:CD008347.
12. Masuda H, Alev C, Akimaru H, Ito R, Shizuno T, Kobori M, Horii M, Ishihara T, Isobe K, Isozaki M, Itoh J, Itoh Y, Okada Y, McIntyre BA, Kato S, Asahara T. Methodological development of a clonogenic assay to determine endothelial progenitor cell potential. *Circ Res*. 2011;109:20–37.
13. Mosser DM, Edwards JP. Exploring the full spectrum of macrophage activation. *Nat Rev Immunol*. 2008;8:958–969.
14. Mosser DM, Zhang X. Interleukin-10: new perspectives on an old cytokine. *Immunol Rev*. 2008;226:205–218.
15. Bartunek J, Vanderheyden M, Vandekerckhove B, Mansour S, De Bruyne B, De Bondt P, Van Haute I, Lootens N, Heyndrickx G, Wijns W. Intracoronary injection of CD133-positive enriched bone marrow progenitor cells promotes cardiac recovery after recenyocardial infarction: feasibility and safety. *Circulation*. 2005;112:I178–I183.
16. Losordo DW, Schatz RA, White CJ, Udelson JE, Veereshwarayya V, Durgin M, Poh KK, Weinstein R, Kearney M, Chaudhry M, Burg A, Eaton L, Heyd L, Thorne T, Shturman L, Hoffmeister P, Story K, Zak V, Dowling D, Traverse JH, Olson RE, Flanagan J, Sodano D, Murayama T, Kawamoto A, Kusano KF, Wollins J, Welt F, Shah P, Soukas P, Asahara T, Henry TD. Intramyocardial transplantation of autologous CD34+ stem cells for intractable angina: a phase I/IIa double-blind, randomized controlled trial. *Circulation*. 2007;115:3165–3172.
17. Kawamoto A, Katayama M, Handa N, Kinoshita M, Takano H, Horii M, Sadamoto K, Yokoyama A, Yamanaka T, Onodera R, Kuroda A, Baba R, Kaneko Y, Tsukie T, Kurimoto Y, Okada Y, Kihara Y, Morioka S, Fukushima M, Asahara T. Intramuscular transplantation of G-CSF-mobilized CD34(+) cells in patients with critical limb ischemia: a phase I/IIa, multicenter, single-blinded, dose-escalation clinical trial. *Stem Cells*. 2009;27:2857–2864.
18. Losordo DW, Henry TD, Davidson C, Sup Lee J, Costa MA, Bass T, Mendelsohn F, Fortuin FD, Pepine CJ, Traverse JH, Amrani D, Ewenstein BM, Riedel N, Story K, Barker K, Povsic TJ, Harrington RA, Schatz RA; Investigators AC. Intramyocardial, autologous CD34+ cell therapy for refractory angina. *Circ Res*. 2011;109:428–436.

19. Kinoshita M, Fujita Y, Katayama M, Baba R, Shibakawa M, Yoshikawa K, Katakami N, Furukawa Y, Tsukie T, Nagano T, Kurimoto Y, Yamasaki K, Handa N, Okada Y, Kuronaka K, Nagata Y, Matsubara Y, Fukushima M, Asahara T, Kawamoto A. Long-term clinical outcome after intramuscular transplantation of granulocyte colony stimulating factor-mobilized CD34 positive cells in patients with critical limb ischemia. *Atherosclerosis*. 2012;224:440–445.
20. Scheubel RJ, Zorn H, Silber RE, Kuss O, Morawietz H, Holtz J, Simm A. Age-dependent depression in circulating endothelial progenitor cells in patients undergoing coronary artery bypass grafting. *J Am Coll Cardiol*. 2003;42:2073–2080.
21. Vasa M, Fichtlscherer S, Aicher A, Adler K, Urbich C, Martin H, Zeiher AM, Dimmeler S. Number and migratory activity of circulating endothelial progenitor cells inversely correlate with risk factors for coronary artery disease. *Circ Res*. 2001;89:E1–E7.
22. Hill JM, Zalos G, Halcox JP, Schenke WH, Waclawiw MA, Quyyumi AA, Finkel T. Circulating endothelial progenitor cells, vascular function, and cardiovascular risk. *N Engl J Med*. 2003;348:593–600.
23. Masuda H, Iwasaki H, Kawamoto A, Akimaru H, Ishikawa M, Ii M, Shizuno T, Sato A, Ito R, Horii M, Ishida H, Kato S, Asahara T. Development of serum-free quality and quantity control culture of colony-forming endothelial progenitor cell for vasculogenesis. *Stem Cells Transl Med*. 2012;1:160–171.
24. Kalka C, Masuda H, Takahashi T, Kalka-Moll WM, Silver M, Kearney M, Li T, Isner JM, Asahara T. Transplantation of ex vivo expanded endothelial progenitor cells for therapeutic neovascularization. *Proc Natl Acad Sci USA*. 2000;97:3422–3427.
25. Hur J, Yoon CH, Kim HS, Choi JH, Kang HJ, Hwang KK, Oh BH, Lee MM, Park YB. Characterization of two types of endothelial progenitor cells and their different contributions to neovasculogenesis. *Arterioscler Thromb Vasc Biol*. 2004;24:288–293.
26. Sasaki K, Heeschen C, Aicher A, Ziebart T, Honold J, Urbich C, Rossig L, Koehl U, Koyanagi M, Mohamed A, Brandes RP, Martin H, Zeiher AM, Dimmeler S. Ex vivo pretreaent of bone marrow mononuclear cells with endothelial NO synthase enhancer AVE9488 enhances their functional activity for cell therapy. *Proc Natl Acad Sci USA*. 2006;103:14537–14541.
27. Pesce M, Orlandi A, Iachininoto MG, Straino S, Torella AR, Rizzuti V, Pompilio G, Bonanno G, Scambia G, Capogrossi MC. Myoendothelial differentiation of human umbilical cord blood-derived stem cells in ischemic limb tissues. *Circ Res*. 2003;93:e51–e62.
28. Napoli C, Williams-Ignarro S, de Nigris F, de Rosa G, Lerman LO, Farzati B, Matarazzo A, Sica G, Botti C, Fiore A, Byrns RE, Sumi D, Sica V, Ignarro LJ. Beneficial effects of concurrent autologous bone marrow cell therapy and metabolic intervention in ischemia-induced angiogenesis in the mouse hindlimb. *Proc Natl Acad Sci USA*. 2005;102:17202–17206.
29. Sica V, Williams-Ignarro S, de Nigris F, D'Armiento FP, Lerman LO, Balestrieri ML, Maione C, Palagiano A, Rossiello L, Ignarro LJ, Napoli C. Autologous bone marrow cell therapy and metabolic intervention in ischemia-induced angiogenesis in the diabetic mouse hindlimb. *Cell Cycle*. 2006;5:2903–2908.
30. Hur J, Yang HM, Yoon CH, Lee CS, Park KW, Kim JH, Kim TY, Kim JY, Kang HJ, Chae IH, Oh BH, Park YB, Kim HS. Identification of a novel role of T cells in postnatal vasculogenesis: characterization of endothelial progenitor cell colonies. *Circulation*. 2007;116:1671–1682.
31. Fadini GP, Albiero M, Boscaro E, Menegazzo L, Cabrelle A, Piliego T, Federici M, Agostini C, Avogaro A. Rosuvastatin stimulates clonogenic potential and anti-inflammatory properties of endothelial progenitor cells. *Cell Biol Int*. 2010;34:709–715.
32. Sica A, Larghi P, Mancino A, Rubino L, Porta C, Totaro MG, Rimoldi M, Biswas SK, Allavena P, Mantovani A. Macrophage polarization in tumour progression. *Semin Cancer Biol*. 2008;18:349–355.
33. Zhang F, Tang Z, Hou X, Lennartsson J, Li Y, Koch AW, Scotney P, Lee C, Arjunan P, Dong L, Kumar A, Rissanen TT, Wang B, Nagai N, Fons P, Fariss R, Zhang Y, Wawrousek E, Tansey G, Raber J, Fong GH, Ding H, Greenberg DA, Becker KG, Herbert JM, Nash A, Yla-Herttuala S, Cao Y, Watts RJ, Li X. VEGF-B is dispensable for blood vessel growth but critical for their survival, and VEGF-B targeting inhibits pathological angiogenesis. *Proc Natl Acad Sci USA*. 2009;106:6152–6157.
34. Gluzman Z, Koren B, Preis M, Cohen T, Tsaba A, Cosset FL, Shofti R, Lewis BS, Virmani R, Flugelman MY. Endothelial cells are activated by angiopoeitin-1 gene transfer and produce coordinated sprouting in vitro and arteriogenesis in vivo. *Biochem Biophys Res Commun*. 2007;359:263–268.
35. Borselli C, Storrie H, Benesch-Lee F, Shvartsman D, Cezar C, Lichan JW, Vandenburgh HH, Mooney DJ. Functional muscle regeneration with combined delivery of angiogenesis and myogenesis factors. *Proc Natl Acad Sci USA*. 2010;107:3287–3292.
36. Johnson C, Sung HJ, Lessner SM, Fini ME, Galis ZS. Matrix metalloproteinase-9 is required for adequate angiogenic revascularization of ischemic tissues: potential role in capillary branching. *Circ Res*. 2004;94:262–268.
37. Shao H, Tan Y, Eton D, Yang Z, Uberti MG, Li S, Schulick A, Yu H. Statin and stromal cell-derived factor-1 additively promote angiogenesis by enhancement of progenitor cells incorporation into new vessels. *Stem Cells*. 2008;26:1376–1384.
38. Tsukada S, Kwon SM, Matsuda T, Jung SY, Lee JH, Lee SH, Masuda H, Asahara T. Identification of mouse colony-forming endothelial progenitor cells for postnatal neovascularization: a novel insight highlighted by new mouse colony-forming assay. *Stem Cell Res Ther*. 2013;4:20.
39. Rohde E, Malischnik C, Thaler D, Maierhofer T, Linkesch W, Lanzer G, Guelly C, Strunk D. Blood monocytes mimic endothelial progenitor cells. *Stem Cells*. 2006;24:357–367.
40. Delorme B, Basire A, Gentile C, Sabatier F, Monsonis F, Desouches C, Blot-Chabaud M, Uzan G, Sampol J, Dignat-George F. Presence of endothelial progenitor cells, distinct from mature endothelial cells, within human CD146+ blood cells. *Thromb Haemost*. 2005;94:1270–1279.
41. Mosser DM, Zhang X. Activation of murine macrophages. *Curr Protoc Immunol*. 2008;Chapter 14:Unit 14.2.
42. Liu G, Yang H. Modulation of macrophage activation and programming in immunity. *J Cell Physiol*. 2013;228:502–512.
43. Dace DS, Khan AA, Kelly J, Apte RS. Interleukin-10 promotes pathological angiogenesis by regulating macrophage response to hypoxia during development. *PLoS One*. 2008;3:e3381.
44. Goetze S, Bungenstock A, Czupalla C, Eilers F, Stawowy P, Kintscher U, Spencer-Hansch C, Graf K, Nurnberg B, Law RE, Fleck E, Grafe M. Leptin induces endothelial cell migration through Akt, which is inhibited by PPARgamma-ligands. *Hypertension*. 2002;40:748–754.
45. Heida NM, Leifheit-Nestler M, Schroeter MR, Muller JP, Cheng IF, Henkel S, Limbourg A, Limbourg FP, Alves F, Quigley JP, Ruggeri ZM, Hasenfuss G, Konstantinides S, Schafer K. Leptin enhances the potency of circulating angiogenic cells via src kinase and integrin (alpha)vbeta5: implications for angiogenesis in human obesity. *Arterioscler Thromb Vasc Biol*. 2010;30:200–206.
46. Rabinovsky ED, Draghia-Akli R. Insulin-like growth factor I plasmid therapy promotes in vivo angiogenesis. *Mol Ther*. 2004;9:46–55.
47. Schomig K, Busch G, Steppich B, Sepp D, Kaufmann J, Stein A, Schomig A, Ott I. Interleukin-8 is associated with circulating CD133+ progenitor cells in acute myocardial infarction. *Eur Heart J*. 2006;27:1032–1037.
48. Krishnamurthy P, Thal M, Verma S, Hoxha E, Lambers E, Ramirez V, Qin G, Losordo D, Kishore R. Interleukin-10 deficiency impairs bone marrow-derived endothelial progenitor cell survival and function in ischemic myocardium. *Circ Res*. 2011;109:1280–1289.
49. Hynes B, Kumar AH, O'Sullivan J, Klein Buneker C, Leblond AL, Weiss S, Schmeckpeper J, Martin K, Caplice NM. Potent endothelial progenitor cell-conditioned media-related anti-apoptotic, cardiotrophic, and pro-angiogenic effects posyocardial infarction are mediated by insulin-like growth factor-1. *Eur Heart J*. 2013;34:782–789.
50. Medina RJ, O'Neill CL, O'Doherty TM, Knott H, Guduric-Fuchs J, Gardiner TA, Stitt AW. Myeloid angiogenic cells act as alternative M2 macrophages and modulate angiogenesis through interleukin-8. *Mol Med*. 2011;17:1045–1055.
51. Tateno K, Minamino T, Toko H, Akazawa H, Shimizu N, Takeda S, Kunieda T, Miyauchi H, Oyama T, Matsuura K, Nishi J, Kobayashi Y, Nagai T, Kuwabara Y, Iwakura Y, Nomura F, Saito Y, Komuro I. Critical roles of muscle-secreted angiogenic factors in therapeutic neovascularization. *Circ Res*. 2006;98:1194–1202.
52. Musaro A, McCullagh K, Paul A, Houghton L, Dobrowolny G, Molinaro M, Barton ER, Sweeney HL, Rosenthal N. Localized IGF-1 transgene expression sustains hypertrophy and regeneration in senescent skeletal muscle. *Nat Genet*. 2001;27:195–200.
53. Pelosi L, Giacinti C, Nardis C, Borsellino G, Rizzuto E, Nicoletti C, Wannenes F, Battistini L, Rosenthal N, Molinaro M, Musaro A. Local expression of IGF-1 accelerates muscle regeneration by rapidly modulating inflammatory cytokines and chemokines. *FASEB J*. 2007;21:1393–1402.
54. Wang M, Tsai B, Brown JW, Meldrum DR. Insulin-like growth factor-1 in myocardial tissue: interaction with tumor necrosis factor. *Crit Care*. 2003;7:417–419.
55. Iekushi K, Seeger F, Assmus B, Zeiher AM, Dimmeler S. Regulation of cardiac microRNAs by bone marrow mononuclear cell therapy in myocardial infarction. *Circulation*. 2012;125:1765–1773, S1761–S1767.

ORIGINAL ARTICLE

JBMR®

SDF-1/CXCR4 Axis in Tie2-Lineage Cells Including Endothelial Progenitor Cells Contributes to Bone Fracture Healing

Yohei Kawakami,[1,2] Masaaki Ii,[3] Tomoyuki Matsumoto,[1,2] Ryosuke Kuroda,[2] Tomoya Kuroda,[1] Sang-Mo Kwon,[5] Atsuhiko Kawamoto,[1] Hiroshi Akimaru,[1] Yutaka Mifune,[1,2] Taro Shoji,[1,2] Tomoaki Fukui,[1,2] Masahiro Kurosaka,[2] and Takayuki Asahara[1,4]

[1]Group of Vascular Regeneration, Institute of Biomedical Research and Innovation, Kobe, Japan
[2]Department of Orthopaedic Surgery, Kobe University Graduate School of Medicine, Kobe, Japan
[3]Department of Pharmacology, Faculty of Medicine, Osaka Medical College, Takatsuki, Japan
[4]Department of Regenerative Medicine Science, Tokai University School of Medicine, Isehara, Japan
[5]Department of Physiology, School of Medicine, Pusan National University, Yangsan, Korea

ABSTRACT

CXC chemokine receptor 4 (CXCR4) is a specific receptor for stromal-derived-factor 1 (SDF-1). SDF-1/CXCR4 interaction is reported to play an important role in vascular development. On the other hand, the therapeutic potential of endothelial progenitor cells (EPCs) in fracture healing has been demonstrated with mechanistic insight of vasculogenesis/angiogenesis and osteogenesis enhancement at sites of fracture. The purpose of this study was to investigate the influence of the SDF-1/CXCR4 pathway in Tie2-lineage cells (including EPCs) in bone formation. We created CXCR4 gene conditional knockout mice using the Cre/loxP system and set two groups of mice: Tie2-Cre^{ER} CXCR4 knockout mice (CXCR4$^{-/-}$) and wild-type mice (WT). We report here that in vitro, EPCs derived from of CXCR4$^{-/-}$ mouse bone marrow demonstrated severe reduction of migration activity and EPC colony-forming activity when compared with those derived from WT mouse bone marrow. In vivo, radiological and morphological examinations showed fracture healing delayed in the CXCR4$^{-/-}$ group and the relative callus area at weeks 2 and 3 was significantly smaller in CXCR4$^{-/-}$ group mice. Quantitative analysis of capillary density at perifracture sites also showed a significant decrease in the CXCR4$^{-/-}$ group. Especially, CXCR4$^{-/-}$group mice demonstrated significant early reduction of blood flow recovery at fracture sites compared with the WT group in laser Doppler perfusion imaging analysis. Real-time RT-PCR analysis showed that the gene expressions of angiogenic markers (CD31, VE-cadherin, vascular endothelial growth factor [VEGF]) and osteogenic markers (osteocalcin, collagen 1A1, bone morphogenetic protein 2 [BMP2]) were lower in the CXCR4$^{-/-}$ group. In the gain-of-function study, the fracture in the SDF-1 intraperitoneally injected WT group healed significantly faster with enough callus formation compared with the SDF-1 injected CXCR4$^{-/-}$ group. We demonstrated that an EPC SDF-1/CXCR4 axis plays an important role in bone fracture healing using Tie2-Cre^{ER} CXCR4 conditional knockout mice. © 2014 American Society for Bone and Mineral Research.

KEY WORDS: FRACTURE HEALING; CX CHEMOKINE RECEPTOR 4 (CXCR4); STROMAL-DERIVED FACTOR-1 (SDF-1); KNOCKOUT MICE; ENDOTHELIAL PROGENITOR CELL (EPC)

Introduction

CXC chemokine receptor 4 (CXCR4) is an alpha chemokine receptor specific for stromal cell-derived-factor 1 (SDF-1)[1] and is endowed with potent chemotactic activity for various lymphocytes.[2] SDF-1/CXCR4 interaction is reported to play an important physiological role during embryogenesis in hematopoiesis,[3,4] vascular development,[5] cardiogenesis,[6,7] and cerebellar development.[8,9] Moreover, the SDF-1/CXCR4 interaction contributes to the regulation of endothelial progenitor cell (EPC) recruitment in ischemic tissues.[10] Locally delivered SDF-1 augments vasculogenesis and subsequently contributes to ischemic neovascularization in vivo by augmenting EPC recruitment in ischemic tissues. Falco and colleagues unraveled a function for SDF-1 in the increase of EPC numbers and in the formation of vascular structures by bone marrow progenitor cells.[11] On the other hand, our group has recently reported that EPCs may play an essential role in fracture healing by promoting a favorable

Received in original form February 11, 2014; revised form June 30, 2014; accepted July 25, 2014. Accepted manuscript online July 31, 2014.
Address correspondence to: Takayuki Asahara, MD, PhD, Group of Vascular Regeneration, Institute of Biomedical Research and Innovation, 2-2 Minatojima-Minamimachi, Chuo-ku, Kobe 650-0047, Japan. E-mail: asa777@is.icc.u-tokai.ac.jp. Masaaki Ii, MD, PhD, Department of Pharmacology, Faculty of Medicine, Osaka Medical College, 2-7, Daigaku-machi, Takatsuki, Osaka 596-8686, Japan. E-mail: masaii@art.osaka-med.ac.jp
Additional Supporting Information may be found in the online version of this article.

Journal of Bone and Mineral Research, Vol. 30, No. 1, January 2015, pp 95–105
DOI: 10.1002/jbmr.2318

environment through neovascularization and osteogenesis in damaged skeletal tissue.[12–15] However, a relationship between the SDF-1/CXCR4 pathway and bone fracture healing is still unclear.

In the process of fracture repair, most fractures heal appropriately in a certain period with callus formation, which bridges the fracture gap while bone repair takes place. However, a significant proportion (5% to 10%) of fractures fail to heal and result in delayed union or persistent nonunion, causing serious problems in the patient's quality of life.[16–19] Therefore, clarification of the process of fracture repair and establishment of a novel therapeutic strategy for nonunion healing and delayed union is clinically warranted in the musculoskeletal field. Among various causes of failed bone formation and remodeling, inappropriate neoangiogenesis is considered to be a crucial factor.[16,18,20,21] The majority of tissues require appropriate vascularization and blood supply to support proper function. Without it, cells suffer from hypoxia, lack of nutrients, accumulation of waste products, and disruption of biomechanical signaling pathways, affecting tissue homeostasis and preventing tissue regeneration.[22] Notably, appropriate vasculogenesis, by bone marrow (BM) EPCs,[23] is emerging as a prerequisite for bone development and regeneration, and we have recently proven the pathophysiological role and benefit in contribution of murine BM-derived Sca1 + Lineage cells, hematopoietic stem cell (HSC)/EPC-enriched fraction for bone healing.[13]

Building from these backgrounds, we speculate that a mechanism of SDF-1/CXCR4 axis in bone fracture healing by EPC recruitment is pivotal. Thus, in the present study, we used a bone fracture model of the Tie2-Cre^{ER} CXCR4 conditional knockout mouse,[24] in which CXCR4 is knocked out specifically in Tie2-expressing endothelial lineage cells. The purpose of this study was to investigate the influence of the SDF-1/CXCR4 pathway on EPCs in the bone formation in vivo and in vitro using CXCR4 conditional knockout mouse and to probe the development of future bone therapy. This is the first study to our knowledge that clarifies the relationship between the SDF-1/CXCR4 pathway in EPC and bone fracture healing.

Materials and Methods

Experimental animals

Wild-type (WT) male C57BL6/J mice (CLEA Japan, Inc., Tokyo, Japan) aged 6 weeks and weighing 25 g to 27 g were used as a control group in this study. The mice were fed a standard maintenance diet and provided water *ad libitum*. All animal procedures were performed in accordance with the Japanese Physiological Society Guidelines for the Care and Use of Laboratory Animals, and the study protocol was approved by the ethical committee of the RIKEN Center for Developmental Biology.

CXCR4 gene silencing

We used the Cre^{ER}/loxP system by generating the tissue-specific CXCR4 gene knockout mice.[25,26] CXCR4$^{lox/flox}$ mice were generated as described previously.[27] The CXCR4-CKO (CXCR4$^{flox/flox}$; Tie2-Cre/+) mice crossed with CXCR4$^{flox/flox}$ mice, resulting in generating the homozygote CXCR4-CKO mice in Tie2-positive cells. Tie2-Cre(+) transgenic mice (C57BL/6J background) were kindly provided by Dr K Hozumi (Department of Immunology, Tokai University School of Medicine, Kanagawa, Japan). To generate the mice in which CXCR4 was inactivated in Tie2-positive cells, the genomic DNA was extracted from mouse tails, according to the manufacturer's instructions (PureLink Genomic DNA Purification Kit, Invitrogen, Carlsbad, CA, USA). After checking the genotype of CXCR4-knockout mice, we intraperitoneally administered tamoxifen (Tm; Sigma, St. Louis, MO, USA; T5648) suspension (75 mg/kg body weight) once per day for 5 days to transgenic mice to activate Cre^{ER} recombinase. We used these CXCR4 conditional knockout (CXCR4$^{-/-}$) mice and WT mice for further experiments. Age- and sex-matched (male) mice were used for all experiments. To confirm the CXCR4 gene silencing, we assessed peripheral blood Tie2-positive (EPC-enriched population) cells of WT and CXCR4$^{-/-}$ mice by fluorescence-activated cell sorting (FACS) analysis (Supplemental Fig. S1*A*). FACS analysis demonstrated that the population of CXCR4-positive cells in peripheral blood Tie2-positive cells was significantly diminished in CXCR4$^{-/-}$ mice. (WT, 17.45%; CXCR4$^{-/-}$, 0.75%, respectively) (Supplemental Fig. S1*B*). Before fracture creation, we performed structural assessment for intact bone between WT mice and CXCR4$^{-/-}$ mice by micro–computed tomography (μCT) and skeletal preparation. We also assessed the influence of tamoxifen on serum estradiol (E2) levels in WT mice and CXCR4KO mice. There was no significant difference between two groups in all parameters (Supplemental Figs. S1*C* and S2, Supplemental Table S1). The details are given in the Supplemental Data.

Mouse EPC culture

BM-derived mouse EPCs (mEPCs) were isolated as described previously with some modifications.[28] Briefly, bone marrow cells collected from all bones of CXCR4$^{-/-}$ mice or WT mice aged 6 weeks were separated by Histopaque-1083 (Sigma) density gradient centrifugation. Light-density mononuclear cells (MNCs) were harvested and washed twice with Dulbecco's phosphate-buffered saline (PBS; no calcium or magnesium; Invitrogen) supplemented with 2 mmol/L EDTA followed by contaminating red blood cell hemolysis by ammonium chloride solution. MNCs were then plated on cell culture dishes coated with rat vitronectin (Sigma, surface concentration 0.47 μg/cm^2) at a density of 5×10^5 cells/mm^2 and cultured in Dulbecco's Modified Eagle Medium (DMEM; Invitrogen) supplemented with 10% fetal bovine serum (FBS; Gibco, Life Technologies, Inc., Carlsbad, CA, USA) and antibiotics. After 24 hours in culture, nonadherent cells were reseeded at a density of 5×10^5 cells/mm^2 in 5% FBS/EBM-2 (Lonza, Basel, Switzerland) medium. After a further 3-day culture, the attached cells were used as the EPC-rich cell population for the following in vitro studies.

EPC colony-forming assay and proliferation and migration assays with mouse EPCs

The EPC colony-forming assay established in our laboratory was performed as reported previously.[29–31] The number of EPC colonies was assessed after culture of each EPC in a 6-well plate for 16 days in methyl cellulose-containing medium M3236 (Stem Cell Technologies, Vancouver, Canada) with 20 ng/mL SCF (Kirin, Tokyo, Japan), 50 ng/mL vascular endothelial growth factor (VEGF; R&D Systems, Minneapolis, MN, USA), 20 ng/mL interleukin-3 (Kirin), and 50 ng/mL basic fibroblast growth factor (bFGF) (Wako, Osaka, Japan). Two different types of attaching cell colonies made of small EPCs and large EPCs were counted separately.

Proliferation activity of mEPC was examined using a Cell Counting Kit-8 (Dojindo Laboratories Inc., Kumamoto, Japan), according to the manufacturer's instructions. Migration activity was evaluated with a modified Boyden's chamber assay as described previously.[32] The details are given in the Supplemental Data.

Bone fracture mouse model

All surgical procedures were performed under anesthesia and normal aseptic conditions. Mice were anesthetized with ketamine hydrochloride (60 mg/kg) and xylazine hydrochloride (10 mg/kg) administered intraperitoneally. An animal model of femoral fracture was applied using a modification of the method described by Manigrasso.[33] All femur fractures were unilateral fractures and unfractured femurs were used as controls for functional analysis. The details are given in the Supplemental Data.

Radiographic assessment for fracture healing

Twenty animals were assigned to each group for radiological observation of the healing process. Radiographs of fractured hind limbs were serially taken at weeks 0, 1, 2, 3, and 4 after creation of fractures under anesthesia with the animals supine and both limbs fully extended. Fracture union was identified by the presence of a bridging callus on two cortices using the criteria proposed by Hammer and colleagues.[34] We applied μCT data together to make doubly sure of its accuracy. Radiographs in each animal were examined by three blinded observers. As a result, we could not find any variability in stage of union and only small variability in sub-items such as point estimates in K values for the Hammer union scale and for the number of cortices bridged by callus. For quantification of callus/trabecular bone formation, μCT imaging analysis was performed on 2, 3, and 4 weeks after fracture creation using X-ray CT system (Latheta LCT-200; Hitachi Aloka Medical, Tokyo, Japan).[35,36] Parameters used for the CT scans were as follows: tube voltage, 50 kVp; tube current, 500 μA; integration time, 3.6 ms; axial field of view, 30 mm with an isotropic voxel size of 30 μm. To evaluate the fracture healing process, relative callus areas around fracture sites in scanned radiographs were quantified using LaTheta software. First, we took soft X-rays to identify the fractured site of the femur using LaTheta software. Next, we scanned a 0.1-mm slice focusing around the fractured site. Using axial images of scanned CT, we marked bony cortex and its external callus area and recognized the callus area as the region of interest (ROI). Then, we set ROI squares on the axial image so that the software could measure its area. We defined the total callus area as the sum of the callus area of each axial image. Bone densities in the callus areas were calculated with CT intensity in scanned images by single-energy X-ray absorptiometry method and averaged using LaTheta software (Hitachi Aloka Medical). A threshold density of 160 mg/cm^3 was selected to distinguish mineralized from unmineralized tissue. The density range was calibrated daily with a manufacturer-supplied phantom. We also applied another μCT (high-resolution scanner viva CT 40, Scanco Medical AG., Brüttisellen, Switzerland) for microarchitectural analyses. Details are shown in the Supplemental Data.

Biomechanical analysis of fracture union

Three mice in each group were used for biomechanical evaluation at weeks 4 after fracture. Biomechanical evaluation was performed in Kureha Special Laboratory (KSL, Tokyo, Japan). Fractured femurs and contralateral nonfractured femurs were prepared and intramedullar fixation pins were removed before the bending test. The standardized three-point bending test was performed using the load torsion and bending tester MZ-500S (Maruto Instruments, Co., Ltd., Tokyo, Japan). The bending force was applied with cross-head at a speed of 2 mm/min until fracture occurred. The extrinsic stiffness (N/mm) and the ultimate stress (N) were interpreted and calculated from the load deflection curve. Ultimate strength was defined as the maximum load sustained during loading, and the ultimate stiffness was defined as the slope of the line extending to the point of maximum sustained torque.[37] The relative ratio of the fractured (right) femur to nonfractured (left) femur was calculated in each group and averaged.

Morphometric evaluation of capillary density and osteoblast density by immunofluorescence staining

To evaluate capillary density and osteoblast (OB) density at the perifracture sites of week 1, immunohistochemistry staining was performed with fluorescent-conjugated isolectin B4 for mouse EC marker (1:100 dilution, Vector Laboratories Inc., Burlingame, CA), or anti-mouse goat osteocalcin (OC) (1:250 dilution, Biogenesis, Poole, U.K.), a marker for mouse OBs. The secondary antibody for OC was Alexa-Fluor 594-conjugated donkey anti-goat IgG (1:1000, Invitrogen). 4′,6-diamino-2-phenylindole (DAPI) solution (1:5000, Sigma-Aldrich) was applied for 5 minutes for nuclear staining. The capillary and OB density was morphometrically evaluated as average values in five randomly selected fields in the soft tissue of perifracture sites under a fluorescent microscope. Capillaries were recognized as tubular structures positive for isolectin B4. OB-like cells were recognized as OC-positive cells on new bone surface. All morphometric studies were performed by two examiners who were blinded to treatment.

Physiological assessment for blood perfusion by laser Doppler imaging

A laser Doppler perfusion imaging (LDPI) system (Moor Instrument, Wilmington, DE, USA)[38,39] was used to measure serial blood flow in both hind limbs at 0, 1, 2, and 3 weeks postfracture, according to the manufacturer's instruction. The ratio of fractured/intact contralateral blood flow was calculated to evaluate the serial blood flow recovery after surgery. The details are given in the Supplemental Data.

Quantitative real-time PCR analysis

Total RNA was obtained from granulation tissues and callus tissues of perifracture site at day 7 using Tri-zol (Life Technologies), according to the manufacturer's instructions. For quantitative real-time RT-PCR, after the first-strand cDNA was synthesized using a RNA LA PCR Kit Ver. 1.1 (Takara Bio Inc., Shiga, Japan), the converted cDNA samples (2 μL) were amplified in triplicate by real-time PCR (ABI PRISM 7700, Applied Biosystems, Carlsbad, CA, USA) in a final volume of 20 μL using SYBR Green Master Mix reagent (Applied Biosystems) with gene-specific primers listed in Supplemental Table S2). Melting curve analysis was performed with Dissociation Curves Software (Applied Biosystems). Results were obtained using sequence detection software (ABI PRISM 7700), and the mean cycle threshold (Ct) values were used to calculate gene expressions with normalization to human or rat glyceraldehydes-3-phosphate (GAPDH). To avoid interspecies cross reactivity of primer pairs between human and mouse genes, we designed mouse-specific primers (CD31, VE-cadherin, VEGF, osteocalcin, collagen1A1, BMP2) using Oligo software (Takara Bio Inc.).

In vivo EPC incorporation assay and immunofluorescent staining

To evaluate EPC incorporation into the fracture site, 1.5×10^5 EPCs derived from the CXCR4$^{-/-}$ or WT group mice were intravenously

injected into the WT fractured mice just after creation of bone fracture. To detect EPC incorporation into the fracture site, transplanted EPCs were labeled with the fluorescent carbocaynine 1,1′-dioctadecyl1-1 to 3,3,3′3′-tetramethylidiocarboyanine perchlorate (Dil) dye (Molecular Probes, Eugene, OR, USA). Before transplantation, EPCs in suspension were washed with PBS and incubated with Dil at a concentration of 2.5 g/mL PBS for 5 minutes at 37°C and 15 minutes at 4°C. After two washing steps in PBS, the cells were resuspended in EBM-2 (Lonza). Historical samples were embedded in OCT compound (Sakura Finetek Japan, Tokyo, Japan), snap-frozen in liquid nitrogen, and cut into 5-μm-thick sections on day 7. Frozen sections of the fracture sites were stained with isolectin B4 (Vector Laboratories) and DAPI to evaluate homing EPCs by counting double staining randomly selected per sample ($n = 5$).

SDF-1 stimulation test

To evaluate gain-of-function of the SDF-1/CXCR4 axis on therapeutic neovascularization and bone healing during fracture repair, we set another two groups of the SDF-1 intraperitoneally injected wild-type group (WT + SDF-1) and SDF-1 intraperitoneally injected $CXCR4^{-/-}$ group (CXCR4 + SDF-1), and studied radiographical and histological assessments after fracture creation compared with the existing WT and $CXCR4^{-/-}$ groups ($n = 20$ each). Immediately after femoral fracture creation described above, one group of mice received an intraperitoneal injection of 20 μg/kg SDF-1. Radiographs of the fractured hind limbs were taken at weeks 0, 1, 2, 3, and 4, and immunohistochemistry staining with fluorescent-conjugated isolectin B4 for mouse EC marker was done at week 1 after creation of fracture as described above.

Statistical analysis

The results were statistically analyzed using a software package (GraphPad Prism, GraphPad Software, Inc., La Jolla, CA, USA). All values were expressed as mean ± SEM. Unpaired *t* tests (Mann-Whitney U test) were performed for comparison between two groups. Multiple comparisons among groups were made using a one-way analysis of variance (ANOVA) followed by post hoc testing with Tukey's procedure. The comparison of radiological results was performed with a chi-square test. A p value <0.05 was considered to denote statistical significance.

Results

Morphological recovery of fractured bone in CXCR4 knockout mice

To evaluate fracture repair morphologically, radiographic and histological examinations were performed. Fractures were united radiographically with bridging callus formation in 55% (11 of 20) of WT mice at week 2 and 85% (17 of 20) at week 3. In contrast, fracture sites of the $CXCR4^{-/-}$ group showed only 30% (6 of 20) fracture healing at week 2 and 60% (12 of 20) at week 3 ($p < 0.05$ in weeks 2 and 3). The time course of union rate in each group is described in Fig. 1*A*.

Morphological and functional fracture healing in each group was further evaluated by μCT at 2, 3 and 4 weeks after fracture surgery. The results of μCT exhibited striking trabecular bone formation in the WT group compared with the $CXCR4^{-/-}$ group at weeks 2 and 3 (2 weeks: WT, 85.80 ± 9.14 versus $CXCR4^{-/-}$, 12.08 ± 1.26 mm^3, $p < 0.001$; 3 weeks: WT, 86.22 ± 7.28 versus $CXCR4^{-/-}$, 39.43 ± 3.64 mm^3, $p < 0.001$, $n = 3$) (Fig. 1*B, C*). In all animals at week 4, callus absorption was found as a general sign of chronic stage of bone healing (4 weeks: WT, 51.78 ± 5.26 versus $CXCR4^{-/-}$, 29.08 ± 5.11 mm^3, $p < 0.05$, $n = 3$) (Fig. 1*C*). Quality of healed bone was also examined using μCT images of week 4 and expressed as bone density, trabecular width, and number of trabeculae. All parameters in the $CXCR4^{-/-}$ group exhibited significantly lower values than in the WT group at week 4 (bone density: WT, 519.60 ± 37.50 versus $CXCR4^{-/-}$, 323.90 ± 30.93, $p < 0.05$; width of trabecular: WT, 32.67 ± 1.14 versus $CXCR4^{-/-}$, 21.12 ± 2.19, $p < 0.05$; number of trabecular: WT, 2.1 ± 0.25 versus $CXCR4^{-/-}$, 0.96 ± 0.19, $p < 0.05$, $n = 3$) (Fig. 1*D–F*).

Decreased functional bone healing after fractures in CXCR4 knockout mice

To confirm functional recovery of the fractured bones, biomechanical evaluation by a three-point bending test was performed at week 4 in both groups ($n = 3$ in each group). There was no significant difference of the specimen length between the WT group and $CXCR4^{-/-}$ group. (WT, 18.8 ± 0.2 versus $CXCR4^{-/-}$, 18.2 ± 0.7 mm, NS). The percentage ratios of extrinsic stiffness and ultimate stress in the fractured femur versus contralateral intact femur were significantly superior in the WT group over the $CXCR4^{-/-}$ group (percent ultimate stress: WT, 68.3 ± 6.3 versus $CXCR4^{-/-}$, 49.3 ± 2.2, $p < 0.05$, $n = 3$; percent extrinsic stiffness: WT, 65.3 ± 4.1 versus $CXCR4^{-/-}$, 47.7 ± 4.2, respectively, $p < 0.05$, $n = 3$) (Fig. 1*G, H*).

Serial deterioration of blood flow recovery at fracture site in CXCR4 knockout mice

To evaluate blood flow recovery via neovascularization at fracture sites, LDPI was serially examined after fracture generation at the fracture site as a physiological approach (Fig. 2*A*). LDPI analysis demonstrated a severe reduction of blood flow 1 hour after fracture in both groups. There was no significant difference in the blood flow ratio of fractured to intact hind limbs 1 hour after fracture creation between both groups (week 0). The blood perfusion ratios were significantly higher in the WT group than the $CXCR4^{-/-}$ group at week 1 (WT, 1.22 ± 0.03 versus $CXCR4^{-/-}$, $1.04 \pm 0.02/mm^2$, $p < 0.05$, $n = 7$), and a similar trend continued until 2 weeks after surgery (WT, 1.19 ± 0.03 versus $CXCR4^{-/-}$, $1.04 \pm 0.08/mm^2$, $p < 0.05$, $n = 7$). At week 3, the blood flow ratio exhibited no significant difference between both groups (Fig. 2*B*).

Decline of intrinsic neoangiogenesis and osteogenesis in the early phase of fracture healing in CXCR4 knockout mice

Toluidine blue staining was performed to address the region of interest where we examined the immunostaining (Fig. 3*A*). An angiogenesis and osteogenesis on the perifracture sites' tissues during the fracture healing were confirmed by immunostaining for mouse-specific markers. Histochemical vascular staining with isolectin B4 (marker for mouse EC) using tissue samples collected 1 week postfracture demonstrated reduced neovascularization around the endochondral ossification area in the $CXCR4^{-/-}$ group animals (WT, 194.3 ± 31.6 versus $CXCR4^{-/-}$, $69.0 \pm 8.0/mm^2$, $p < 0.001$, $n = 5$) (Fig. 3*B, D*). OB staining with anti-mouse OC on tissue samples collected 1 week postfracture revealed the augmentation of osteogenesis in the newly formed bone area in the WT group mice compared with the $CXCR4^{-/-}$ group mice (WT, 235.0 ± 13.6 versus $CXCR4^{-/-}$, $116.0 \pm 9.0/mm^2$, $p < 0.001$, $n = 5$) (Fig. 3*C, E*).

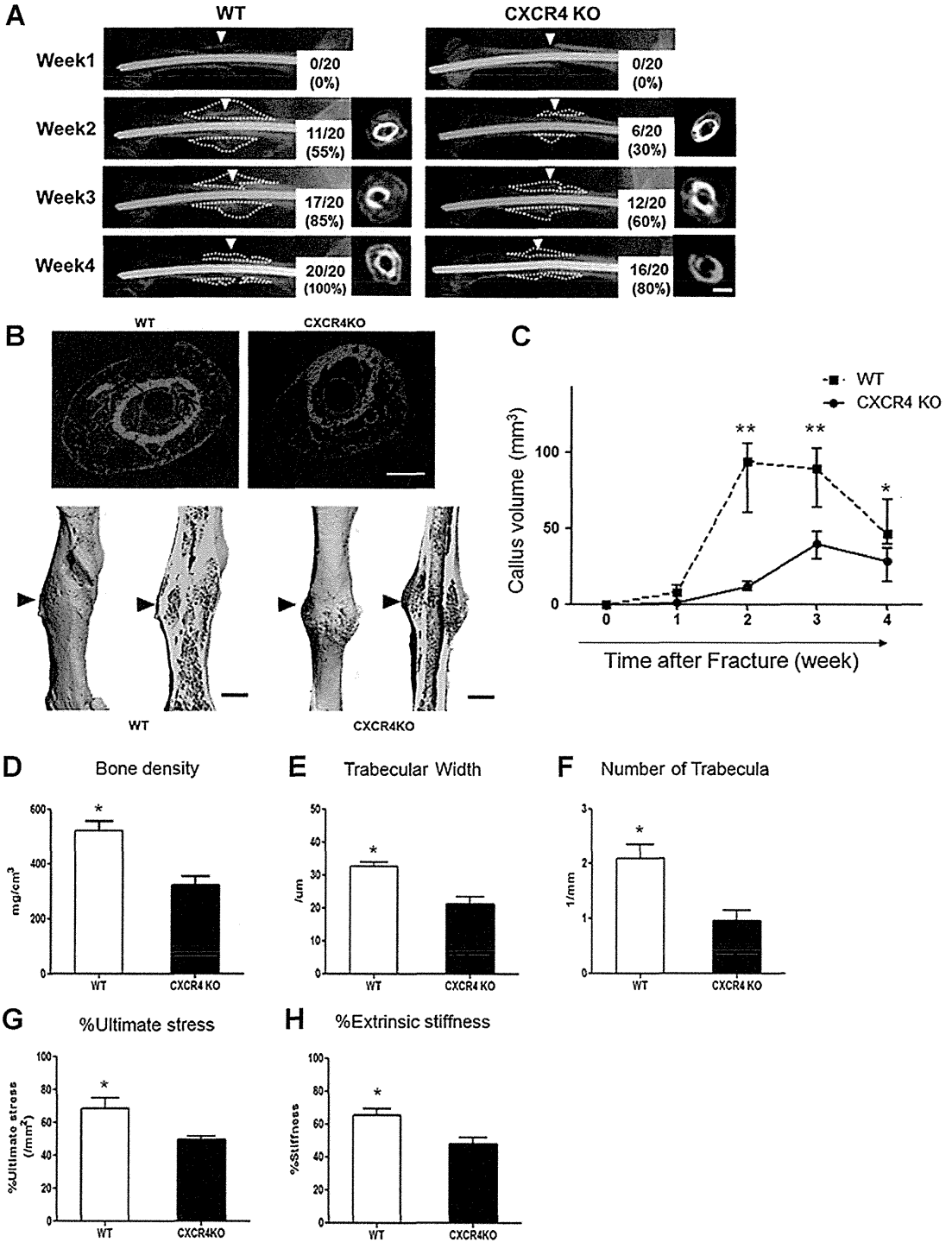

Fig. 1. Radiological and functional assessments for fracture healing. (*A*) Representative radiographs and μCT axial images of fracture sites at weeks 1, 2, 3, and 4 in each group ($n = 20$ in each group and at each time point). (*B*) High-magnification and 3D reconstruction images of μCT at week 3. Arrowheads show fracture sites in femurs. White dotted lines show bridging callus formation. Scale bar = 1 mm (*A, B*). Quantitative μCT analysis of fracture healing. Callus volume (*C*), bone density (*D*), width trabeculae (*E*), and number of trabeculae (*F*) at week 4 were quantified in the μCT images and averaged. $^{**}p < 0.001$ (*C*) and $^{*}p < 0.05$ (*D–F*). Functional recovery after fracture is assessed by biomechanical three-point bending test at week 4. Percentage of each parameter for ultimate stress (*G*) and extrinsic stiffness (*H*) indicates the ratio of each value in the fracture site to the contralateral intact femur ($n = 3$ in each group and each parameter). $^{*}p < 0.05$.

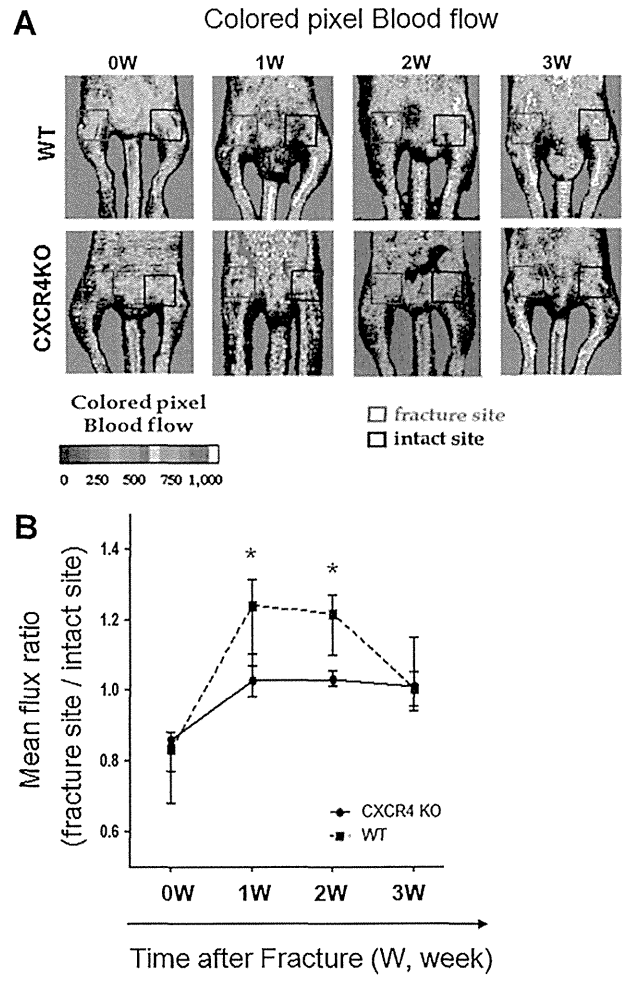

Fig. 2. Assessment for blood flow recovery in sites of fracture. (*A*) Representative LDPI at weeks 0 (1 hour after fracture), 1, 2, and 3 are shown. In these digital color-coded images, maximum perfusion values are indicated in white to red, medium values in green to yellow, and lowest values in dark blue. (*B*) Quantitative analyses of local blood perfusion. The blood flow within the fracture site (red square) and intact contralateral site (black square) were evaluated as mean flux, and the ratio of the mean flux in the fractured site to that in the contralateral site (mean flux ratio) was expressed as relative blood perfusion of fracture site. $^{*}p < 0.05$.

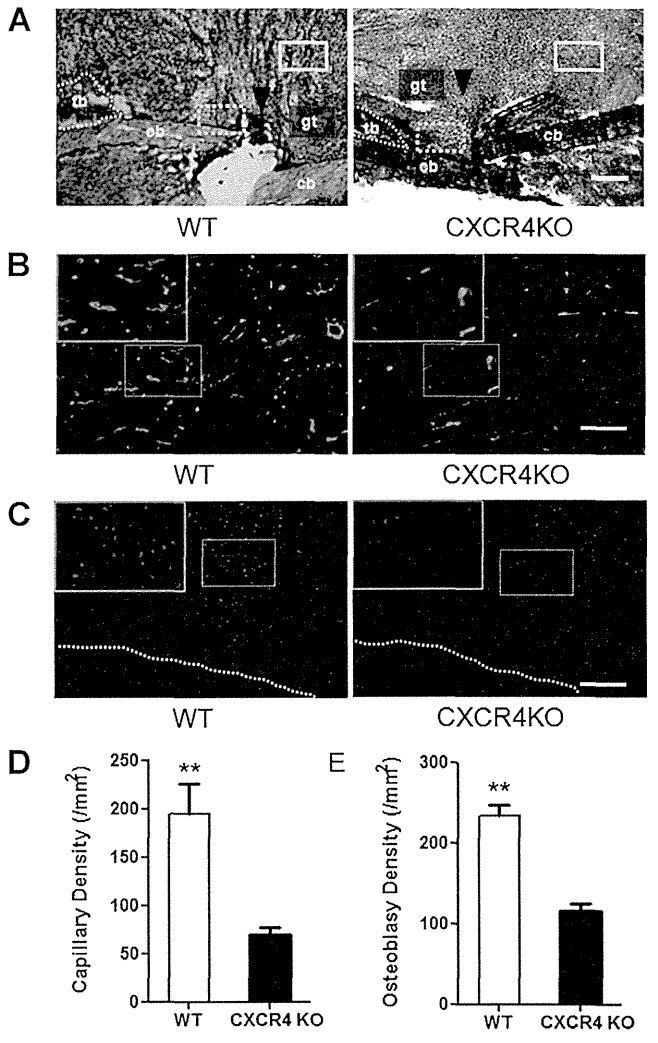

Fig. 3. Assessment for morphology, angiogenesis, and osteogenesis in sites of fracture. (*A*) Representative toluidine blue staining at week 1. White dotted lines mark the edge of callus formation. Arrowheads show the sites of femur fracture. The area surrounded by yellow squares indicates the region of interest observed by vascular staining. The area surrounded by yellow dotted squares marks the region of interest observed by ostaoblast staining. Scale bar = 300 μm. cb = cortical bone; gt = granulation tissue; tb = trabecular bone. (*B*) Representative vascular staining with isolectin B4 (green) and DAPI (blue) using tissue samples of perifracture sites collected at week 1 in both groups. (*C*) Representative osteoblast staining with anti-mouse osteocalcin (red) and DAPI (blue) using tissue samples of perifracture sites collected at week 1 in both groups. Original magnification ×100; scale bar = 100 μm. Left upper panels in each image (*B, C*) indicate high-magnification images of the area surrounded by white dotted squares. Original magnification ×200. White dotted lines mark the edge of cortical bone. (*D, E*) Quantification of capillaries and osteoblasts. Isolectin B4-positive capillaries (*D*) and OC-positive osteoblasts (*E*) were counted in five randomly selected high-power fields and averaged ($n = 5$ in each group). $^{**}p < 0.001$.

Molecules for vasculogenesis and osteogenesis reduced at fracture site in CXCR4$^{-/-}$ mice

To explore the underlying mechanism by which intrinsic angiogenesis and osteogenesis declined in the CXCR4$^{-/-}$ group mice, we assessed mRNA expressions of pro-angiogenic and -osteogenic cytokines in tissue RNA isolated from the perifracture sites 1 week after surgery by real-time RT-PCR, quantifying the expression of mouse vascular endothelial cadherin (mVE-cad), mCD31, mouse vascular endothelial growth factor (mVEGF), mOC, mouse collagen 1 alpha 1 (mCol1A1), and mouse bone morphogenetic protein-2 (mBMP-2). The results demonstrated a significantly higher expression of angiogenic markers (CD31, VE-cad, VEGF) to GAPDH in the WT group compared with the CXCR4$^{-/-}$ group (mCD31: WT, 1009.0 ± 76.6 vs. CXCR4$^{-/-}$, 202.2 ± 38.5, $p < 0.05$, mVE-cad: WT, 1998.0 ± 245.8 vs. CXCR4$^{-/-}$, 701.9 ± 143.3, $p < 0.05$, mVEGF: WT, 11846.0 ± 423.5vs. CXCR4$^{-/-}$, 3641.0 ± 327.6, $p < 0.05$, $n = 5$) (Fig. 4*A–C*).

The relative mRNA expression of bone-related markers (mOC, mCol1A1, and mBMP-2) to mGAPDH were significantly higher in the WT group compared with the CXCR4$^{-/-}$ group (mOC: WT,

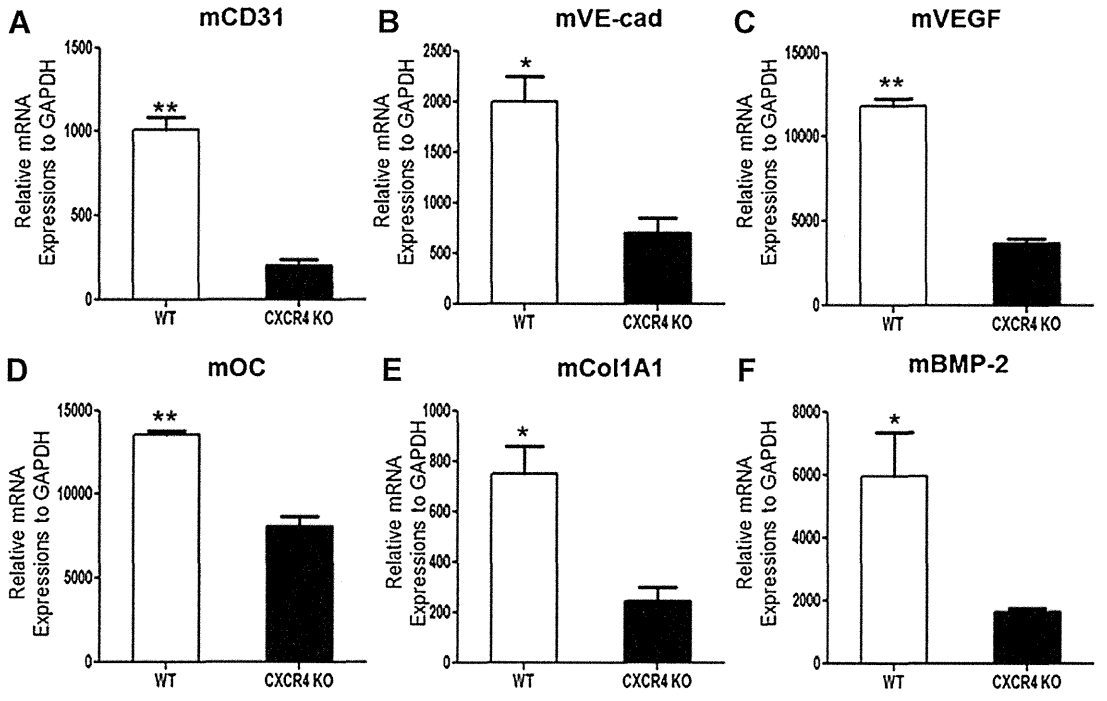

Fig. 4. Angiogenic and osteogenic gene expression in sites of fracture. Total RNA was extracted from perifracture tissue 1 week after surgery and examined the indicated mRNA expressions by quantitative real-time RT-PCR analysis ($n = 5$ in each group). The relative expression levels of mouse-specific CD31 (*A*), VE-cad (*B*), VEGF (*C*), OC (*D*), Col1A1 (*E*), and BMP-2 (*F*) to mGAPDH are expressed in the graphs. $^{*}p < 0.05$ and $^{**}p < 0.001$.

13452.0 ± 241.9 versus CXCR4$^{-/-}$, 8049.0 ± 658.8, $p < 0.05$; mCol1-A1: WT, 750.6 ± 108.9 versus CXCR4$^{-/-}$, 244.6 ± 54.2, $p < 0.05$; mBMP2: WT, 5942.0 ± 1418.0 versus CXCR4$^{-/-}$, 1624.0 ± 105.8, $p < 0.05$, $n = 5$) (Fig. 4*D–F*).

CXCR4$^{-/-}$ EPC incorporation into sites of fracture reduced

To determine the effect of SDF-1/CXCR4 axis on the homing capacity of putative EPCs' incorporation into bone fracture sites, we intravenously infused DiI-labeled EPCs into WT mice immediately after creation of bone fracture. The expression of SDF-1 is upregulated at the fractured site and ischemic site. Staining for EPCs revealed significantly abundant incorporation of labeled EPCs, which derived from WT mice into fracture sites. In contrast, very few EPCs that were derived from CXCR4$^{-/-}$ mice were incorporated into the fractured site (WT, 18.8 ± 1.5 versus CXCR4$^{-/-}$, 2.2 ± 0.9 cells/view field, $p < 0.001$, $n = 5$) (Fig. 5*A, B*).

CXCR4$^{-/-}$ EPCs exhibited low capacity of colony formation and impairment of migration ability in vitro

To evaluate the function as EPCs in vitro, cells were analyzed by EPC colony-forming assay. After 16 days in culture with a methylcellulose-based medium, the average number of small EPC colonies per dish of the CXCR4$^{-/-}$ group was significantly smaller than that of the WT group (small colony: CXCR4$^{-/-}$, 19.4 ± 0.5 versus WT, 28.0 ± 1.8, $p < 0.05$; large colony: CXCR4$^{-/-}$, 2.2 ± 0.4 versus WT, 3.0 ± 0.3, $p =$ NS, $n = 5$) (Fig. 5*C, D*). Each EPC colony-formation unit showed a differentiation hierarchy from small EPC to large EPC colonies, indicating a primitive EPC stage with high proliferative activity and a definitive EPC stage with vasculogenic properties, respectively.

The proliferation activities of CXCR4$^{-/-}$ mice– and WT mice–derived mEPC were expressed as a mean optical density value at a wavelength of 490 nm. CXCR4$^{-/-}$mice–derived mEPCs showed depression of proliferation activities compared with WT-derived mEPCs (CXCR4$^{-/-}$, 0.68 ± 0.05 versus WT, 0.84 ± 0.03, $p < 0.05$, $n = 8$) (Fig. 5*E*). The migration activities of mEPCs were evaluated using a Transwell culture plate, and mEPCs migrated toward SDF-1a containing medium were evaluated as the activity. CXCR4$^{-/-}$ mice–derived mEPCs demonstrated significant weakening in migration activities of mEPCs (CXCR4$^{-/-}$, 166.40 ± 8.52 versus WT, 56.63 ± 9.08, $p < 0.001$, $n = 8$) (Fig. 5*F*).

SDF-1 treatment failed to improve functional recovery after fracture in CXCR4$^{-/-}$ mice

To investigate role of SDF-1 in CXCR4-deficient mice, the gain-of-function test of SDF-1 on bone fracture healing processes was confirmed by radiograph and histological examination. In radiographical study, fractures were united with bridging callus formation in 70% (14 of 20) of the WT + SDF1 group mice at week 2 and 95% (19 of 20) at week 3. In contrast, fracture sites of the CXCR4$^{-/-}$ + SDF1 group showed only 40% (8 of 20) fracture healing at week 2 and 65% (13 of 20) at week 3. The acceleration of fracture healing was found in between WT and WT + SDF1 groups ($p < 0.05$ in weeks 2 and 3). In contrast, there was no significant difference between the CXCR4$^{-/-}$ and CXCR4$^{-/-}$ + SDF1 groups. The time course of union rate in each group is described in Fig. 6*A*.

The results of μCT exhibited striking trabecular bone formation in the WT + SDF1 group compared with the WT group at weeks 2 and 3. Moreover, relative callus area at week 2 was significantly greater in the SDF-1–administered WT group than in other

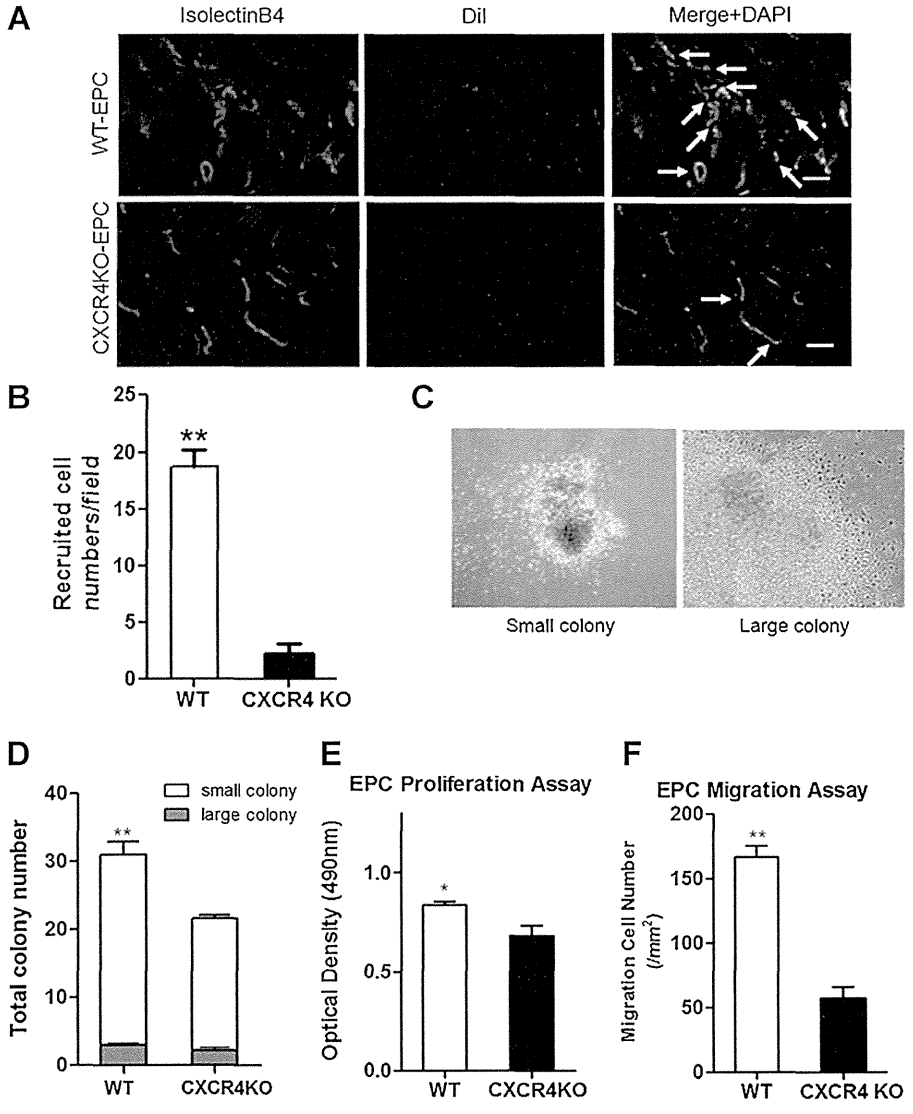

Fig. 5. EPC functions and EPC recruitment to fracture site. (*A*) In vivo EPC recruitment assay. Representative microscopic photographs of double fluorescence in perifracture sites at day 7. Transplanted DiI-labeled EPCs were identified by red fluorescence in histological sections retrieved from perifracture capillaries. Host mouse capillaries were identified by isolectin B4 (green fluorescence). DAPI (blue) was used for nuclear staining. Arrows indicate recruited DiI-positive transplanted EPCs. Scale bar = 100 μm. (*B*) Quantitative analysis for the recruited EPCs was performed and expressed as a density of DiI-labeled EPCs (red fluorescence) in tissue sections retrieved from perifracture sites. $^{**}p < 0.001$. (*C, D*) Colony-forming assay of EPCs in vitro. (*C*) Representative images of a small colony and a large colony. Scale bar = 100 μm. (*D*) Average numbers of large EPC colonies and small EPC colonies per dish were expressed as colony-forming activity. $^{**}p < 0.001$. (*E, F*) Proliferation and migration activities of EPCs. (*E*) The proliferation activity is expressed as optical density (490 nm). (*F*) The migration activity is expressed as the number of migrated cells to SDF-1. $^{*}p < 0.05$ and $^{**}p < 0.001$.

groups. On the other hand, SDF1 injection was effective only at week 2 in the $CXCR4^{-/-}$ group, and there was no significant difference between the $CXCR4^{-/-}$ group and the $CXCR4^{-/-}$ + SDF1 group at any other time points. (2 weeks: WT + SDF1, 117.9 ± 5.7 versus WT, 85.8 ± 9.1, $p < 0.05$; $CXCR4^{-/-}$ + SDF1, 23.8 ± 4.9 versus $CXCR4^{-/-}$, 12.1 ± 1.3 mm^3, p = NS; 3 weeks: WT + SDF1, 125.2 ± 4.4 versus WT, 86.2 ± 7.3, $p < 0.05$, $CXCR4^{-/-}$ + SDF1, 26.1 ± 5.0 versus $CXCR4^{-/-}$, 39.4 ± 3.6 mm^3, p = NS, $n = 3$) (Fig. 6*B*). In all animals at week 4, callus absorption was found as a general sign of chronic stage of bone healing.

In histological analysis, serial vascular staining with isolectin B4 at week 1 demonstrated enhanced neovascularization around the endochondral ossification area in the WT + SDF1 group. In contrast, there was no significant difference between the $CXCR4^{-/-}$ group and the $CXCR4^{-/-}$ + SDF1 group (WT + SDF1, 272.0 ± 42.4; WT, 194.3 ± 31.6; $CXCR4^{-/-}$ + SDF1, 66.8 ± 17.7; $CXCR4^{-/-}$, 69.0 ± 16.1; WT + SDF1 versus WT, $p < 0.05$, $CXCR4^{-/-}$ versus $CXCR4^{-/-}$ + SDF1, p = NS, $n = 5$) (Fig. 6*C, D*).

Discussion

In the present study, we demonstrated that fracture healing delayed and formed callus diminished in CXCR4-deficient mice compared with wild-type mice. An attenuation of angiogenesis and osteogenesis at fracture site in CXCR4-deficient mice could

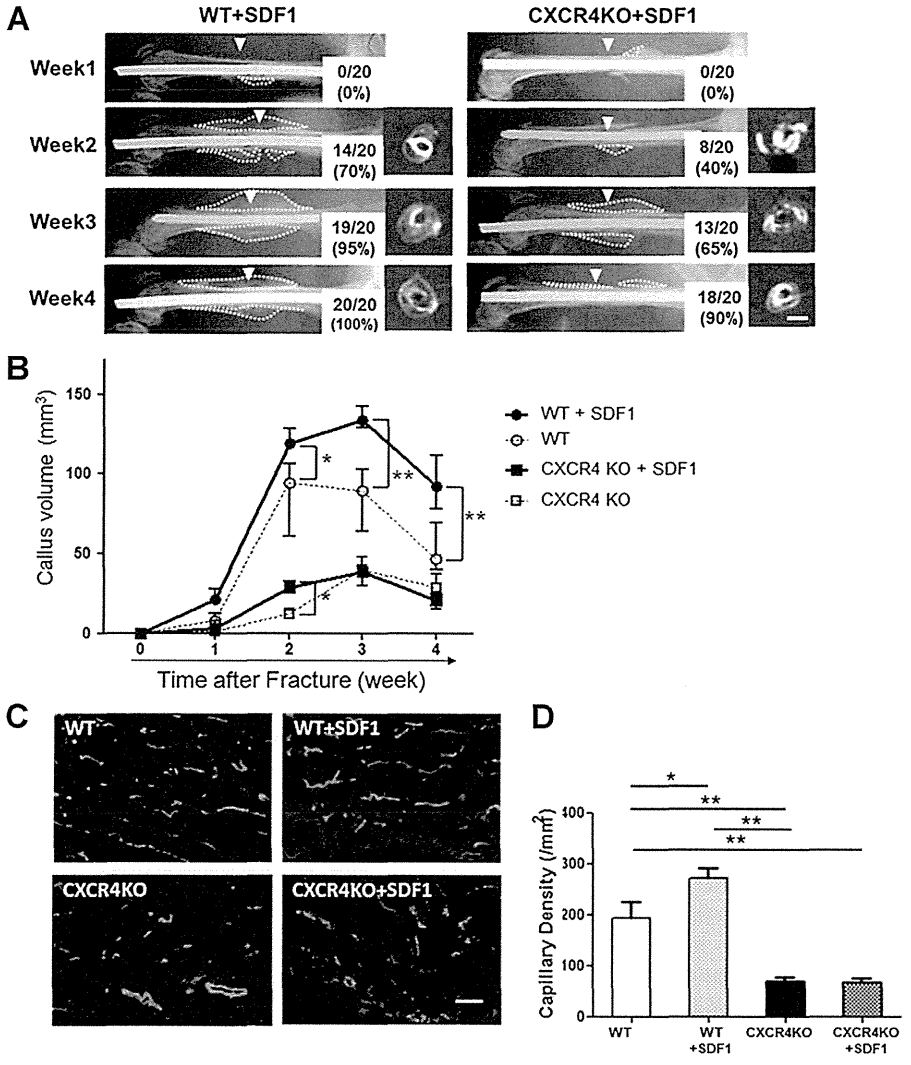

Fig. 6. Gain-of-function test by SDF-1 administration to WT mice and CXCR4$^{-/-}$ mice with fracture. (*A*) Representative radiographs and μCT axial images of fracture sites at weeks 1, 2, 3, and 4 in each group ($n = 20$ in each group and at each time point). White dotted lines show bridging callus formation. Scale bar = 100 μm; arrowheads show sites of femur fracture. (*B*) μCT analysis for fracture healing. Callus volumes were quantified in the μCT images and averaged. *$p < 0.05$ and **$p < 0.001$. (*C*) Representative vascular staining with isolectin B4 (green) and DAPI (blue) using tissue samples of perifracture sites collected at week 1 in each group. Magnification ×100 in; scale bar = 100 μm. (*D*) Quantification of capillaries. Isolectin B4-positive capillaries were counted in five randomly selected high-power fields and averaged ($n = 5$ in each group). *$p < 0.05$ and **$p < 0.001$.

be considered a cause of this impair in fracture repair. First, we showed the effect of CXCR4 knockout in vivo. Normally, mice lacking the CXCR4 gene die perinatally because of the abnormality in their hematopoietic system.[8] In our study, we made an adult conditional CXCR4$^{-/-}$ murine model using the Cre/loxP system. The result of both quantitative histochemical analysis for capillary density and LDPI test indicates that a lack of CXCR4 led to reduced blood flow in the CXCR4$^{-/-}$ group mice during fracture repair. Quantitative RT-PCR analysis also revealed the reasonable decrease of angiogenesis-related markers in CXCR4$^{-/-}$ mice at the molecular level. Moreover, EPC incorporation study demonstrated that EPCs derived from CXCR4$^{-/-}$ mice could not accumulate to the fractured site properly because of their impairment of the migration ability to SDF-1. Our in vitro data also indicate that EPCs derived from CXCR4$^{-/-}$ mice lose their migration ability to SDF-1 and their colony formation abilities are weakened. These results support the hypothesis that the SDF-1/CXCR4 axis including mobilization and incorporation of EPCs is an important mechanism for bone fracture healing.[40,41]

Although the physiological role of EPCs in fracture healing remains to be clarified, we have begun to characterize the role of mobilized BM-derived EPCs on fracture healing. We have found that neovascularization is the process of fracture healing during the early phase of endochondral ossification. In the fracture site, there is a significant increase in cell population derived from infiltrating EPC cells. We previously reported that EPCs mobilize into a fracture site before healing by mapping this migration after the systemic administration of peripheral blood (PB) EPCs green fluorescent protein (GFP) + cells into an animal. These findings indicate that fracture may induce the mobilization of EPCs from the BM to fracture site, by way of transport through the PB as a way to augment neovascularization and ultimately bone healing. As supportive data, systemic delivery of EPCs developed a favorable environment for fracture healing by enhancing angiogenesis and osteogensis.[13,42,43]

We speculate that the mechanism of EPCs homing to the fracture site deeply relayed to the SDF-1/CXCR4 axis. It is a known fact that the SDF-1 is upregulated at the fracture site and ischemic site.[10,44] Therefore, EPCs expressing CXCR4 receptor homing to the SDF-1–stimulated fracture site is a reasonable hypothesis. SDF-1/CXCR4 axis contributes to the regulation of EPC recruitment in ischemic tissues.[10] In the present study, we demonstrated that EPCs derived from $CXCR4^{-/-}$ mice could not accumulate to the fractured site properly because of the impairment in their migration ability to SDF-1 in the EPC incorporation study. This data also supported our hypothesis that the SDF-1/CXCR4 axis plays an important role in fracture healing. These findings provide a possible explanation for reduced vasculogenesis/angiogenesis and osteogenesis in $CXCR4^{-/-}$ mice, leading to the delay of fracture healing partly owing to scanty EPC homing to the fracture site. Another group reported SDF-1/CXCR4 axis is also critical for recruitment of mesenchymal stem cells (MSCs) to the fracture site during skeletal repair. Kitaori and colleagues mentioned that SDF-1 is induced in the periosteum of injured bone and promotes endochondral bone repair by recruiting mesenchymal stem cells to the site of injury.[44] Our SDF-1 stimulation test demonstrated that the fracture in the SDF-1–injected WT group healed faster with enough bridging callus and significant abundant new blood vessel formation than the WT group. Previous study also indicates that SDF-1 injection improves the local blood perfusion in a WT mouse hind limb ischemia model.[10] However, there was a limited SDF-1 effect in the $CXCR4^{-/-}$ group. These results indicate that the SDF-1 stimulation effect is more striking in WT mice than $CXCR4^{-/-}$ mice because SDF-1 stimulates all CXCR4-expressing cells in WT mice, whereas SDF-1 does not stimulate Tie2-positive cells in $CXCR4^{-/-}$ mice.

Despite the promising initial results indicating that EPC SDF-1/CXCR4 axis plays an important role in bone fracture healing, there is a certain issue that needs to be resolved before we move to clinical application. Our radiographical assessment disclosed that the callus was developed and fracture healed at week 4 in spite of CXCR4 gene absence. This fact indicates that bone fracture healing is regulated by not only the SDF-1/CXCR4 axis but also other multiple mechanisms.[45,46] Indeed, there might be several other regulatory pathways that are responsible for the bone fracture healing. In the current study, we could find the difference between the $CXCR4^{-/-}$ and $CXCR4^{-/-}$ + SDF groups in radiographical assessments at week 2. Zhu and colleagues reported co-requirement of the SDF1/CXCR4 axis in BMP2-induced osteogenic differentiation of mesenchymal C2C12 and ST2 cells,[47] and Otsuru and colleagues reported the possibility of endogenous circulating marrow-derived osteoblast progenitor cells (MOPCs) contributing to ectopic bone formation[48] and circulating bone marrow–derived osteoblast progenitor cells recruited in bone formation via a SDF-1/CXCR4 axis.[49] In addition to it, Tie2-positive cells including not only EPCs but also other types of cells (subsets of hematopoietic stem cells and monocytes/macrophages)[24] have also been involved in the fracture healing process. However, the relationship between the SDF-1/CXCR4 axis and bone fracture healing is still unclear. Nevertheless, our data shown in this study clearly indicate that the SDF1/CXCR4 axis also regulates EPC incorporation into the fracture site and that the reduced vasculogenesis that led to a delay in fracture healing is partly owing to less EPC homing capacity to the fracture site in $CXCR4^{-/-}$ mice.

In conclusion, this is the first report to our knowledge in which EPC SDF-1/CXCR4 axis has been shown to be an important factor for fracture repair using CXCR4 conditional knockout mice. Moreover, the promotion of EPC SDF-1/CXCR4 axis leads to the acceleration of bone fracture healing and might be served as a novel therapeutic application for genetic bone diseases and bone injuries.

Disclosures

All authors state that they have no conflicts of interest.

Acknowledgments

We thank to Dr Yoichio Iwakura and Dr Bungil Choi for preparing the knockout mice. We also thank the animal facility of RIKEN Center for Developmental Biology for providing the space to perform animal surgery. We thank Ms Kathy Trim for her editing assistance in manuscript preparation.

Authors' roles: TA and MI are corresponding authors and directed the study. YK is the first author. Study design: TA, IM, KS, TM, and YK. Study conduct: YK, HA, and TK. Data collection: YK, TK, ST, and HA. Data interpretation: YK, TK, HA, YM, TF, TS, RK, and MK. Drafting manuscript: YK and MI. All authors discussed the results and their implications and commented on the manuscript.

References

1. Nagasawa T, Kikutani H, Kishimoto T. Molecular cloning and structure of a pre-B-cell growth-stimulating factor. Proc Natl Acad Sci USA. 1994;91(6):2305–9.
2. Kucia M, Jankowski K, Reca R, et al. CXCR4-SDF-1 signalling, locomotion, chemotaxis and adhesion. J Mol Histol. 2004;35(3):233–45.
3. Onai N, Zhang Y, Yoneyama H, Kitamura T, Ishikawa S, Matsushima K. Impairment of lymphopoiesis and myelopoiesis in mice reconstituted with bone marrow-hematopoietic progenitor cells expressing SDF-1-intrakine. Blood. 2000;96(6):2074–80.
4. Nagasawa T, Hirota S, Tachibana K, et al. Defects of B-cell lymphopoiesis and bone-marrow myelopoiesis in mice lacking the CXC chemokine PBSF/SDF-1. Nature. 1996;382(6592):635–8.
5. Chen T, Bai H, Shao Y, et al. Stromal cell-derived factor-1/CXCR4 signaling modifies the capillary-like organization of human embryonic stem cell-derived endothelium in vitro. Stem Cells. 2007;25(2):392–401.
6. Gupta SK, Pillarisetti K. Cutting edge: CXCR4-Lo: molecular cloning and functional expression of a novel human CXCR4 splice variant. J Immunol. 1999;163(5):2368–72.
7. Tachibana K, Hirota S, Iizasa H, et al. The chemokine receptor CXCR4 is essential for vascularization of the gastrointestinal tract. Nature. 1998;393(6685):591–4.
8. Zou YR, Kottmann AH, Kuroda M, Taniuchi I, Littman DR. Function of the chemokine receptor CXCR4 in haematopoiesis and in cerebellar development. Nature. 1998;393(6685):595–9.
9. Hodohara K, Fujii N, Yamamoto N, Kaushansky K. Stromal cell-derived factor-1 (SDF-1) acts together with thrombopoietin to enhance the development of megakaryocytic progenitor cells (CFU-MK). Blood. 2000;95(3):769–75.
10. Yamaguchi J, Kusano KF, Masuo O, et al. Stromal cell-derived factor-1 effects on ex vivo expanded endothelial progenitor cell recruitment for ischemic neovascularization. Circulation. 2003;107(9):1322–8.
11. De Falco E, Porcelli D, Torella AR, et al. SDF-1 involvement in endothelial phenotype and ischemia-induced recruitment of bone marrow progenitor cells. Blood. 2004;104(12):3472–82.
12. Matsumoto T, Kuroda R, Mifune Y, et al. Circulating endothelial/skeletal progenitor cells for bone regeneration and healing. Bone. 2008;43(3):434–9.

13. Matsumoto T, Mifune Y, Kawamoto A, et al. Fracture induced mobilization and incorporation of bone marrow-derived endothelial progenitor cells for bone healing. J Cell Physiol. 2008;215(1):234–42.
14. Mifune Y, Matsumoto T, Kawamoto A, et al. Local delivery of granulocyte colony stimulating factor-mobilized CD34-positive progenitor cells using bioscaffold for modality of unhealing bone fracture. Stem Cells. 2008;26(6):1395–405.
15. Kawakami Y, Ii M, Alev C, et al. Local transplantation of ex vivo expanded bone marrow-derived CD34 positive cells accelerates fracture healing. Cell Transplant. 2012;21(12):2689–709.
16. Colnot CI, Helms JA. A molecular analysis of matrix remodeling and angiogenesis during long bone development. Mech Dev. 2001; 100(2):245–50.
17. Gerstenfeld LC, Cullinane DM, Barnes GL, Graves DT, Einhorn TA. Fracture healing as a post-natal developmental process: molecular, spatial, and temporal aspects of its regulation. J Cell Biochem. 2003;88(5):873–84.
18. Marsh D. Concepts of fracture union, delayed union, and nonunion. Clin Orthop Relat Res. 1998;355(Suppl):S22–30.
19. Rodriguez-Merchan EC, Forriol F. Nonunion: general principles and experimental data. Clin Orthop Relat Res. 2004; (419):4–12.
20. Lu C, Miclau T, Hu D, Marcucio RS. Ischemia leads to delayed union during fracture healing: a mouse model. J Orthop Res. 2007;25(1):51–61.
21. Matsumoto T, Kawamoto A, Kuroda R, et al. Therapeutic potential of vasculogenesis and osteogenesis promoted by peripheral blood CD34-positive cells for functional bone healing. Am J Pathol. 2006;169(4):1440–57.
22. Folkman J. Angiogenesis. Annu Rev Med. 2006;57:1–18.
23. Asahara T, Murohara T, Sullivan A, et al. Isolation of putative progenitor endothelial cells for angiogenesis. Science. 1997; 275(5302):964–7.
24. Kisanuki YY, Hammer RE, Miyazaki J, Williams SC, Richardson JA, Yanagisawa M. Tie2-Cre transgenic mice: a new model for endothelial cell-lineage analysis in vivo. Dev Biol. 2001;230(2):230–42.
25. Araki K, Araki M, Miyazaki J, Vassalli P. Site-specific recombination of a transgene in fertilized eggs by transient expression of Cre recombinase. Proc Natl Acad Sci USA. 1995;92(1):160–4.
26. Bouvard C, De Arcangelis A, Dizier B, et al. Tie2-dependent knockout of alpha6 integrin subunit in mice reduces post-ischaemic angiogenesis. Cardiovasc Res. 2012;95(1):39–47.
27. Chung SH, Seki K, Choi BI, et al. CXC chemokine receptor 4 expressed in T cells plays an important role in the development of collagen-induced arthritis. Arthritis Res Ther. 2010;12(5):R188.
28. Ii M. Bone marrow-derived endothelial progenitor cells: isolation and characterization for myocardial repair. Methods Mol Biol. 2010;660: 9–27.
29. Kwon SM, Eguchi M, Wada M, et al. Specific Jagged-1 signal from bone marrow microenvironment is required for endothelial progenitor cell development for neovascularization. Circulation. 2008;118(2):157–65.
30. Masuda H, Alev C, Akimaru H, et al. Methodological development of a clonogenic assay to determine endothelial progenitor cell potential. Circ Res. 2011;109(1):20–37.
31. Tsukada S, Kwon SM, Matsuda T, et al. Identification of mouse colony-forming endothelial progenitor cells for postnatal neovascularization: a novel insight highlighted by new mouse colony-forming assay. Stem Cell Res Ther. 2013;4(1):20.
32. Shoji T, Ii M, Mifune Y, et al. Local transplantation of human multipotent adipose-derived stem cells accelerates fracture healing via enhanced osteogenesis and angiogenesis. Lab Invest. 2010; 90(4):637–49.
33. Manigrasso MB, O'Connor JP. Characterization of a closed femur fracture model in mice. J Orthop Trauma. 2004;18(10):687–95.
34. Hammer RR, Hammerby S, Lindholm B. Accuracy of radiologic assessment of tibial shaft fracture union in humans. Clin Orthop Relat Res. 1985; (199):233–8.
35. Kawao N, Tamura Y, Okumoto K, et al. Plasminogen plays a crucial role in bone repair. J Bone Miner Res. 2013;28(7):1561–74.
36. Makino Y, Takahashi Y, Tanabe R, et al. Spatiotemporal disorder in the axial skeleton development of the Mesp2-null mouse: a model of spondylocostal dysostosis and spondylothoracic dysostosis. Bone. 2013;53(1):248–58.
37. Fukui T, Ii M, Shoji T, et al. Therapeutic effect of local administration of low-dose simvastatin-conjugated gelatin hydrogel for fracture healing. J Bone Miner Res. 2012;27(5):1118–31.
38. Linden M, Sirsjo A, Lindbom L, Nilsson G, Gidlof A. Laser-Doppler perfusion imaging of microvascular blood flow in rabbit tenuissimus muscle. Am J Physiol. 1995;269(4 Pt 2):H1496–500.
39. Wardell K, Jakobsson A, Nilsson GE. Laser Doppler perfusion imaging by dynamic light scattering. IEEE Trans Biomed Eng. 1993;40(4):309–16.
40. Granero-Molto F, Weis JA, Miga MI, et al. Regenerative effects of transplanted mesenchymal stem cells in fracture healing. Stem Cells. 2009;27(8):1887–98.
41. Cho SW, Sun HJ, Yang JY, et al. Transplantation of mesenchymal stem cells overexpressing RANK-Fc or CXCR4 prevents bone loss in ovariectomized mice. Mol Ther. 2009;17(11):1979–87.
42. Laing AJ, Dillon JP, Condon ET, et al. A systemic provascular response in bone marrow to musculoskeletal trauma in mice. J Bone Joint Surg Br. 2007;89(1):116–20.
43. Lee DY, Cho TJ, Kim JA, et al. Mobilization of endothelial progenitor cells in fracture healing and distraction osteogenesis. Bone. 2008;42(5):932–41.
44. Kitaori T, Ito H, Schwarz EM, et al. Stromal cell-derived factor 1/CXCR4 signaling is critical for the recruitment of mesenchymal stem cells to the fracture site during skeletal repair in a mouse model. Arthritis Rheum. 2009;60(3):813–23.
45. Grewal TS, Genever PG, Brabbs AC, Birch M, Skerry TM. Best5: a novel interferon-inducible gene expressed during bone formation. Faseb J. 2000;14(3):523–31.
46. Moutsatsos IK, Turgeman G, Zhou S, et al. Exogenously regulated stem cell-mediated gene therapy for bone regeneration. Mol Ther. 2001;3(4):449–61.
47. Zhu W, Boachie-Adjei O, Rawlins BA, et al. A novel regulatory role for stromal-derived factor-1 signaling in bone morphogenic protein-2 osteogenic differentiation of mesenchymal C2C12 cells. J Biol Chem. 2007;282(26):18676–85.
48. Otsuru S, Tamai K, Yamazaki T, Yoshikawa H, Kaneda Y. Bone marrow-derived osteoblast progenitor cells in circulating blood contribute to ectopic bone formation in mice. Biochem Biophys Res Commun. 2007;354(2):453–8.
49. Otsuru S, Tamai K, Yamazaki T, Yoshikawa H, Kaneda Y. Circulating bone marrow-derived osteoblast progenitor cells are recruited to the bone-forming site by the CXCR4/stromal cell-derived factor-1 pathway. Stem Cells. 2008;26(1):223–34.

Physiological Reports

Open Access

Physiological Reports ISSN 2051-817X

ORIGINAL RESEARCH

Dextran induces differentiation of circulating endothelial progenitor cells

Syotaro Obi[1], Haruchika Masuda[1], Hiroshi Akimaru[2], Tomoko Shizuno[1], Kimiko Yamamoto[3], Joji Ando[4] & Takayuki Asahara[1,2]

1 Department of Regenerative Medicine Science, Tokai University School of Medicine, Isehara, Japan
2 Vascular Regeneration Research Group, Institute of Biomedical Research and Innovation, Kobe, Japan
3 Department of Biomedical Engineering, Graduate School of Medicine, University of Tokyo, Tokyo, Japan
4 Laboratory of Biomedical Engineering, School of Medicine, Dokkyo Medical University, Tochigi, Japan

Keywords
Culture, endothelial progenitor cell, signal transduction, transcription.

Correspondence
Takayuki Asahara, 143 Shimokasuya, Isehara, Kanagawa, 259-1193, Japan.
Tel: 0463-93-1121
Fax: 0463-95-0961
E-mail: asa777@is.icc.u-tokai.ac.jp

Funding Information
This study was supported in part by a grant-in-aid for Scientific Research on Priority Areas from the Japanese Ministry of Education, Culture, Sports, Science and Technology and by a research grant from the Japanese Ministry of Health, Labor and Welfare.

Received: 7 January 2014; Revised: 17 February 2014; Accepted: 17 February 2014

doi: 10.1002/phy2.261

Physiol Rep, 2 (3), 2014, e00261, doi: 10.1002/phy2.261

Abstract

Endothelial progenitor cells (EPCs) have been demonstrated to be effective for the treatment of cardiovascular diseases. However, the differentiation process from circulation to adhesion has not been clarified because circulating EPCs rarely attached to dishes in EPC cultures previously. Here we investigated whether immature circulating EPCs differentiate into mature adhesive EPCs in response to dextran. When floating-circulating EPCs derived from ex vivo expanded human cord blood were cultured with 5% and 10% dextran, they attached to fibronectin-coated dishes and grew exponentially. The bioactivities of adhesion, proliferation, migration, tube formation, and differentiated type of EPC colony formation increased in EPCs exposed to dextran. The surface protein expression rate of the endothelial markers vascular endothelial growth factor (VEGF)-R1/2, VE-cadherin, Tie2, ICAM1, VCAM1, and integrin αv/β3 increased in EPCs exposed to dextran. The mRNA levels of VEGF-R1/2, VE-cadherin, Tie2, endothelial nitric oxide synthase, MMP9, and VEGF increased in EPCs treated with dextran. Those of endothelium-related transcription factors ID1/2, FOXM1, HEY1, SMAD1, FOSL1, NFkB1, NRF2, HIF1A, EPAS1 increased in dextran-treated EPCs; however, those of hematopoietic- and antiangiogenic-related transcription factors TAL1, RUNX1, c-MYB, GATA1/2, ERG, FOXH1, HHEX, SMAD2/3 decreased in dextran-exposed EPCs. Inhibitor analysis showed that PI3K/Akt, ERK1/2, JNK, and p38 signal transduction pathways are involved in the differentiation in response to dextran. In conclusion, dextran induces differentiation of circulating EPCs in terms of adhesion, migration, proliferation, and vasculogenesis. The differentiation mechanism in response to dextran is regulated by multiple signal transductions including PI3K/Akt, ERK1/2, JNK, and p38. These findings indicate that dextran is an effective treatment for EPCs in regenerative medicines.

Introduction

Endothelial cells have ability of cell division and migration not only in embryo but also in adult life. When a part of endothelium is injured and detached, neighboring endothelial cells proliferate, migrate, and cover the exposed surface. Furthermore, endothelial cells always regenerate and new blood vessels are made in hypoxic lesions. Endothelial progenitor cells (EPCs) are also demonstrated to play an important role for the vascular regeneration (Asahara et al. 1997). EPCs are mobilized from bone marrow to peripheral blood, attach to existing endothelial cells nearby hypoxic lesions, transmigrate into tissues, proliferate, differentiate, secret angiogenic factors, and induce neovascularization (Jujo et al. 2008; Kirton and Xu 2010).

Since the discovery of EPCs, various methods to identify and isolate EPCs have been used (Fadini et al. 2008; Yoder 2009; Pearson 2010), this is because EPCs are thought to exist in the broad process of differentiation between

hemangioblasts and mature endothelial cells. Recently immature EPCs are defined as circulating blood cells which form EPC colonies (Masuda et al. 2011). These colony-forming EPCs are derived from hematopoietic stem cells (HSCs) population and express surface antigens such as CD34, CD133, vascular endothelial growth factor receptor 2 (VEGF-R2, also called Flk1 or KDR), c-Kit, and protein receptor tyrosine kinase, epithelial-specific Tie2 (Asahara et al. 2011). Along with differential processes, colony-forming EPCs lose immature markers and acquire other endothelial or monocyte markers, such as vascular endothelial cadherin (VE-cadherin), E-selectin, integrin αv/β3, and CD14. Then EPCs move onto a non-colony-forming EPC stage. These differentiating EPCs transform from circulating phenotype in suspended manner into tissue phenotype in attached manner after homing to ischemic or regenerative organs. However, the differentiation process from circulation to adhesion has not been clarified because floating-circulating EPCs rarely attached to dishes in EPC cultures previously. The development of adhesion assay by a new technology is needed and would provide deeper insight into the molecular and physiological mechanisms at successive stages of EPC differentiation.

Dextran is a high molecular weight polymer of D-glucose and it is produced by enzymes on the cell surface of certain lactic acid bacteria. It is used commonly to decrease vascular thrombosis. Dextran reduces the activity of factor VIII antigen (von Willebrand factor) and impairs the platelet adhesiveness (Aberg and Rausing 1978; Batlle et al. 1985; Robless et al. 2002). Dextran also increases the plasminogen activity, decreases the α2 antiplasmin activity, and inhibits the fibrin stabilization, thereby it increases the lysis of plasma clots (Carlin and Saldeen 1980; Wieslander et al. 1986a,b). Moreover, dextran is used to reduce blood viscosity and expand blood volume in bleeding. A basic research reported that dextran regulates bioactivities of endothelial cells. Dextran increased endothelial cell viability and decreased leukocyte adhesion to endothelial cells (Rouleau et al. 2010). In addition, dextran increased both protein and mRNA expression levels of intercellular adhesion molecule 1 (ICAM1) and vascular cell adhesion molecule 1 (VCAM1) and caused the nuclear translocation of nuclear factor kappa B (NFκB). These results indicate that dextran influences various molecules and cells, however, the effect of dextran on EPCs remains unknown.

In this regard, we speculate that the exposure of dextran may regulate the biology of not only mature endothelial cells but also immature EPCs derived from bone marrow microenvironments in vivo. Here, we investigated whether dextran influences biological circulating EPCs in a suspension culture. Moreover, we investigated the signal transduction pathways in response to dextran in these EPCs.

Materials and Methods

Materials

Dextran (MW 100,000–200,000; Sigma-Aldrich, D4876) was weighed, dissolved in M199 medium, and filtered through a polyvinylidene difluoride membrane with a pore size of 0.45 μm (Whatman). The viscosity of dextran was measured with a rotating-cone-plate-type viscometer, BIORHEOLIZER (Tokimec) at a constant temperature of 37°C. Measurements were taken over a range of shear rates to verify the Newtonian behavior of the solutions. The viscosity of 0, 5, and 10% dextran in M199 medium were 0.0108, 0.0350, and 0.0794 Poise, respectively. The osmotic pressure of dextran was measured with a cryoscopic osmometer, OSMOMAT 030 (Gonotec). The osmotic pressure of 0, 5, and 10% dextran in M199 medium were 272, 277, and 284 mOsmol/kg, respectively.

The signal transduction inhibitors used were as follows, 10 μmol/L LY294002 (Cell Signaling), 10 μmol/L PD98059 (Calbiocem, La Jolla, CA), 10 μmol/L JNK inhibitor II (Calbiocem), and 10 μmol/L SB203580 (Calbiocem).

Isolation and preparation of human CD133-positive cells

The protocol used in this study was approved by the Tokai University research ethics committee, Japan, and written informed consent was obtained from all participants. Human CD133-positive cells were prepared from freshly obtained human umbilical cord blood after normal delivery as follows. Umbilical cord blood mononuclear cells were isolated by density gradient centrifugation of buffy coats using histopaque1077 (Sigma-Aldrich, St. Louis, MO). CD133-positive cells were purified from the mononuclear cells using anti-CD133 monoclonal antibody-conjugated microbeads (Miltenyi Biotec) and a magnetically activated cell sorter (auto-MACS; Miltenyi Biotec, Bergisch Gladbach, Germany) following the manufacturer's protocol. To confirm the purity of CD133-positive cells, the enriched CD133-positive cells were used in cytometric analyses using a FACS Calibur flow cytometer (BD Biosciences, San Jose, CA). The isolated cells contained approximately 99% pure CD133-positive cells. The isolated CD133-positive cells were resuspended with freezing medium (CELLBANKER; Zenoaq) and were cryopreserved until use.

Ex vivo suspension culture of EPCs

Freshly isolated EPCs were expanded as follows. 3×10^5 CD133-positive cells were cultured at 37°C under 5% CO_2 atmosphere in Stem Span media (StemCell Technologies) with 50 ng/mL vascular endothelial growth

factor (VEGF; R&D Systems, Minneapolis, MN), 20 ng/mL interleukin-6 (R&D Systems), 100 ng/mL stem cell factor (Kirin), 20 ng/mL thrombopoietin (Wako), 100 ng/mL fms-related tyrosine kinase 3 ligand (Wako), and 1% Penicillin/Streptomycin (Invitrogen, Carlsbad, CA) in suspended manner for 7 days. The surface protein expression rates of ex vivo expanded EPCs were analyzed by flow cytometry. The expression rates of CD133, CD34, c-Kit, and CD31 were 40.0 ± 10.4%, 50.2 ± 12.5%, 46.9 ± 19.6%, and 88.8 ± 8.6%, respectively. To confirm the EPC activity, they were incubated with 1,1′-dioctadecyl-3,3,3′,3′-tetramethylindo-carbocyanine perchlorate-labeled acetylated LDL (DiI-acLDL; 1 μg/mL; Biomedical Technologies, Stoughton, MA) at 37°C for 6 h. All cells showed positive staining for DiI-acLDL. This indicates that ex vivo expanded EPCs keep approximately half of the characteristics of freshly isolated EPCs and have an endothelial phenotype. 3×10^4/cm^2 ex vivo expanded EPCs were applied on culture dishes coated with 100 μg/mL solution of human fibronectin (GIBCO, Grand island, NY), and cultured in M199 medium (GIBCO) with 5% fetal bovine serum (FBS; JRH), and EGM2 (VEGF, fibroblast growth factor-2, epidermal growth factor, insulin-like growth factor-1, and ascorbic acid; Clonetics) at 37°C under 5% CO_2 atmosphere for 7 days.

Adhesion assay

2×10^4 EPCs under a dextran-free condition and exposed to 5% and 10% dextran for 24 h were seeded onto a human fibronectin-coated 96-well culture dish in M199 medium with 1% FBS. After incubation in a 5% CO_2 incubator for 5 h, non-adherent cells were removed by gently washing twice with phosphate buffered saline (PBS). The adhesive cells were examined under a phase contrast microscope (ECLIPSE TE300, Nikon, Yurakucho, Japan) equipped with a digital camera DSL1 (Nikon), the images (x10) were imported as JPEG files into National Institutes of Health (NIH) Image software. The number of adhesion cells was measured per each image.

Migration assay

A modified Boyden chamber assay was performed. Using a 24 well-transwell plate with 5 μm pore size polycarbonate membranes (Corning Costar, Acton, MA), M199 medium was in the bottom chamber, and 5×10^4 EPCs under a dextran-free condition and exposed to 10% dextran for 24 h were seeded in the upper chamber coated with fibronectin. The migrated cells through the upper chamber were fixated with VECTASHIELD including 4′, 6-diamino-2-phenylindole (DAPI; Vector) and were counted under a fluorescence microscope (×4) (IX70, Olympus, Shibuya, Japan).

Proliferation assay

The cleavage amount of tetrazolium salt to formazan by cellular mitochondrial dehydrogenase was measured. 1×10^5 EPCs under a dextran-free condition and exposed to 5% and 10% dextran for 24 h were seeded to each well of fibronectin-coated 96-well plates and cultured in M199 medium with 5% FBS for 24 h. Thereafter, the cell proliferation assay reagent WST-1 (Roche Applied Science, Mannheim, Germany) was added and incubated for 5 h. Absorbance at 450 nm was measured using SpectraMax 250 microplate reader (Molecular Devices, Sunnyvale, CA) and Softmax Pro (Molecular Devices).

Tube formation

2×10^3 EPCs under a dextran-free condition and exposed to 10% dextran for 24 h and 1.5×10^4 human umbilical vein endothelial cells (HUVECs) were applied in EBM-2 medium (Lonza, Basel, Switzerland) with 2% FBS, added to an equivalent amount of Matrigel (BD Falcon) in a 96 well-plate. After incubation at 37°C in an atmosphere of 5% CO_2 gels were observed by using a phase contrast microscope (×4). The number of circles per tube structure was counted in each image.

EPC colony-forming assay

5×10^3 EPCs under a dextran-free and exposed to 10% dextran for 24 h were applied in methylcellulose-containing M3236 medium (StemCell Technologies, Vancouver, Canada) with 20 ng/mL stem cell factor (Kirin), 50 ng/mL VEGF (R&D Systems), 20 ng/mL interleukin-3 (Kirin), 50 ng/mL basic fibroblast growth factor (Wako), 50 ng/mL epidermal growth factor (Wako), 50 ng/mL insulin-like growth factor-1 (Wako), and 2 U/mL heparin (Ajinomoto) in a 3 cm-dish. After 15 days in culture, the number of small or large type EPC colonies in a dish was counted under a phase contrast microscope.

Real-time PCR analysis

Total RNA samples were prepared from cells with RNeasy Mini Kit (Qiagen, Valencia, CA), and first-strand cDNAs were generated using a PrimeScript RT reagent Kit (Takara, Ohtsu, Japan). After reverse transcription of the RNA into cDNA, real-time polymerase chain reaction (PCR) was used to monitor gene expression with a 7500 Fast Real-Time PCR System (Applied Biosystems, Foster City, CA) and a SDS 7900 (Applied Biosystems) according

to standard procedures. PCR was performed with a TaqMan Fast Universal PCR Master Mix or SYBR Green PCR Master Mix (Applied Biosystems), and primer pairs and TaqMan probes for VEGF, purchased from Applied Biosystems, vascular endothelial growth factor receptor 1 (VEGF-R1, also called Flt1), VEGF-R2, VE-cadherin, Tie2, endothelial nitric oxide synthase (eNOS), matrix metalloproteinase 9 (MMP9), inhibitor of DNA binding 1 (ID1), ID2, forkhead box m1 (FOXM1), FOXH1, hairy/enhancer of split related with yrpw motif 1 (HEY1), mothers against decapentaplegic, drosophila, homolog of, 1 (SMAD1), SMAD2, SMAD3, fos-like antigen 1 (FOSL1), NFkB1, nuclear factor erythroid 2-related factor 2 (NRF2), hypoxia-inducible factor 1, alpha subunit (HIF1A), endothelial pas domain protein 1 (EPAS1), t-cell acute lymphocytic leukemia 1 (TAL1), runt-related transcription factor 1 (RUNX1), GATA-binding protein 1 (GATA1), GATA2, v-ets avian erythroblastosis virus e26 oncogene homolog (ERG), hematopoietically expressed homeobox (HHEX), and glyceraldehyde-3-phosphate dehydrogenase (GAPDH), respectively (Table 1). Other analyzed genes were listed as below; v-ets avian erythroblastosis virus e26 oncogene homolog 1 (ETS1), ETS2, ets variant gene 2 (ETV2), ETV6, friend leukemia virus integration 1 (FLI1), elk3, ets-domain protein (ELK3), e74-like factor 1 (ELF1), ELF2, ELF3, FOXC1, FOXC2, FOXO1, FOXO3, FOXO4, FOXF1, sry-box 7 (SOX7), SOX17, SOX18, mads box transcription enhancer factor 2, polypeptide a (MEF2A), MEF2C, GATA3, GATA4, ID3, vasculae endothelial zinc finger 1 (VEZF1), krüppel-like c2/h2 zinc-finger transcription factor 2 (KLF2), KLF4, KLF5, lim domain only 2 (LMO2), heart-and neural crest derivatives-expressed 2 (HAND2), HEY2, hairy/enhancer of split, drosophila, homolog of 1 (HES1), homeobox a9 (HOXA9), HOXB3, HOXD3, HOXD10, peroxisome proliferator-activated receptor gamma (PPARG), aryl hydrocarbon receptor nuclear translocator (ARNT), nuclear receptor subfamily 2, group f, member 2 (NR2F2), glioma-associated oncogene homolog (GLI1), gli-kruppel family member 2 (GLI2), GLI3, transcription factor 4 (TCF4), lymphoid enhancer-binding factor 1 (LEF1), SMAD4, SMAD5, early growth response 1 (EGR1), speci-

Table 1. Oligonucleotide primers and probes used for gene expression analysis by real-time PCR.

	Primer Sequences, 5′-3′		
Gene	Forward	Reverse	Probe (5′-FAM, 3′-BHQ)
VEGF-R1	GCATGATGGGAATAGGGAGACA	CCAAGGCCCACTTGATCTTTAG	AGGAAAGGGCGCCTACTCTTCAGG
VEGF-R2	AATGCGGGAGGTTCAATGTG	GGGAAGAACAAAAGGGTAAAATCC	AGCTGTGTGTGGTGTCAAAGTTTCAGG
VE-cadherin	GAGCCGAGCCATGTGTCTTT	GGTGTGCCTGAGGGTCAGTT	None
Tie2	CTGTATACCCTCTGTTTCCCTTTCA	TTGGCAGAGGGCATGTTTTCTC	None
eNOS	CAGCAACGCTACCACGAAGA	TGCGTATGCGGCTTGTCA	ATTTTCGGGCTCACGCTGCG
MMP9	CCCGGAGTGAGTTGAACCA	AGGGCACTGCAGGATGTCA	TGGACCAAGTGGGCTACGTGACCT
ID1	AGAACCGCAAGGTGAGCAA	CCAACTGAAGGTCCCTGATGTAG	TGGAGATTCTCCAGCACGTCATCG
ID2	GGGAGCGAAAACGTTAAAATCA	*ATTCACGCTCCACCTTTGAAA*	*TTGCCCAATCTAAGCAGACTTTGCCTT*
FOXM1	GTACCTGGATCTTGGGTTCTTCA	CAAAAAGGACTCTGGCAAGCA	TGCAGGGACCCAGACAAGTGGA
FOXH1	AGGGCTGAGCCTGGAATAGC	ACGGCTGGTGACTGATGGAT	TTCCTAGTCCCCTCTTCTCAGCCCA
HEY1	TGGTGGCCCTGAATCCAT	GGCTCTCTCCTAACTAAATCAGAACTG	TGACCAGCTGCTGGTATCTGCCA
SMAD1	GTTCTGCAGCTGGTTAATTCATGT	CAAGCACTCCATATAACTGGTATTG	CTGTGAGAGCAAATGAATAATTCCTGC
SMAD2	GAGGAAATACATGGCCTTTGATG	*CTGGCTTCTCGAGCAGAACAG*	*TCTGGCGTCTACTGCATTTCCCAG*
SMAD3	GTGGCTTTTTGGCTCAGCAT	ACACGCGGCCACTTGTTT	CAGAAACACCAAACCAGGCTGGC
FOSL1	CCACACTCTCCATCACCCTCTT	TGGGTAAAGTGGCACCTTCTG	TGTGATCCACCCAACCCTATCTCCTG
NFkB1	TTGTCCCTCTGCTACGTTCCTATT	TGCTGTGGTCAGAAGGAATGC	TCATTAAAGGTATCACGGTCGCCACC
NRF2	CTCAGCACCTTATATCTCGAAGTTTTC	TGCAGGGAGTATTCACTAGGAGAA	CATGCTACGTGATGAAGATGGAAAACCT
HIF1A	*TTGTGGAAGTTTATGCTAATATTGTGTAAC*	*TCTTGTTTACAGTCTGCTCAAAATATCTT*	*TAAACCTAAATGTTCTGCCTACCCTGTTGG*
EPAS1	GTGACATGTAGGTAGGAAGCACTGA	CCAGAGGTGTCGTCCCTCTTAC	AATAGTGTTCCCAGAGCACTTTGCAACTC
TAL1	CAACTCTTTCGGCCTTTTGG	GTCTTCAGCAGAGGGTCACGTA	TGGGTCTGGCCGTACTTGTGATTTC
RUNX1	CCCCCACCTAGGGTCTATTTG	ACGCACGAATTTTCAGGATGT	TGGCAGTTATTGGGTTTGGTCACAA
c-MYB	GCCAGTCACTGCCTTAAGAACA	GCAGTAAGTACACCGTCATATCTCAAA	TTGATGCAAGATGGCCAGCACTG
GATA1	*GGAAGGATGGTATTCAGACTCGAA*	*GACTGGAGCCCCGTTTCTTT*	*CGCAAGGCATCTGGAAAAGGGA*
GATA2	CGTGTCCCGAGCTTAGATTCTG	GCCCATATTGCACTTGGTCACT	CCCAGGAGGAGGATTGTGCTGATG
ERG	CACTGCTTCTCCTAAGCCTTCTG	TCTGCTGCACCTGCTGTCA	ACAGATGTGGCACCTGCAACCC
HHEX	CCACTTAATGGAAAGGCAAAGG	AAATACTCCAAGGCTGCCTGAA	TACCCCAAATCCAGAGGTGCCTACA
GAPDH	GGTGGTCTCCTCTGACTTCAACA	GTGGTCGTTGAGGGCAATG	ACACCCACTCCTCCACCTTTGACG

eNOS, endothelial nitric oxide synthase; VEGF, vascular endothelial growth factor.

ficity protein 1 (SP1), v-jun avian sarcoma virus 17 oncogene homolog (JUN), and v-myc avian myelocytomatosis viral oncogene homolog (MYC). The temperature profile consisted of initial denaturation for 20 sec at 95°C, followed by 40 cycles of denaturation at 95°C for 3 sec, annealing and elongation at 62°C for 30 sec, and fluorescence monitoring at 60°C. The specificity of the amplification reaction was determined by performing a standard curve analysis and a melting curve analysis. Relative signal quantification was achieved by normalizing the signal of each gene to that of the GAPDH gene.

Flow cytometry

Endothelial progenitor cells were washed with cold PBS and were resuspended in PBS with FcR blocking reagent (MACS), 0.2% FBS, and 2 mmol/L EDTA at 4°C for 30 min. They were stained with monoclonal antibodies specific for the following surface antigens: CD34 (Becton Dickinson, San Jose, CA), CD51/61 (integrin αv/β3; Becton Dickinson), CD54 (ICAM1; Becton Dickinson), CD106 (VCAM1; Becton Dickinson), CD117 (c-Kit; MACS), CD133 (MACS), CD144 (VE-cadherin; Beckman Coulter, Brea, CA), CD202b (Tie2; R&D), CD309 (VEGF-R2; R&D), and VEGF-R1 (R&D). After incubation at 4°C for 30 min they were washed twice and were analyzed using two-color flow cytometry.

Statistical analysis

All results are expressed as means ± SD. Statistical significance was evaluated by ANOVA and a Bonferonni adjustment applied to the results of a *t* test performed with SPSS software. *P*-values of <0.05 were regarded as statistically significant.

Results

Culture of circulating EPCs in dextran

Floating EPCs were cultured to investigate whether dextran affects the morphological phenotype of EPCs. EPCs without dextran rarely attached to fibronectin-coated dishes (Fig. 1A). On the other hand, EPCs with 5% dextran began to attach and became elongated at 4 days after seeding. Then, the adhesive EPCs increased at 7 days. Furthermore, adhesive EPCs with 10% dextran increased more exponentially than those with 5% dextran.

Dextran increases bioactivities of adhesion and proliferation

An adhesion assay was performed to investigate whether dextran affects the adhesion of floating EPCs. The exposure of dextran to floating EPCs for 24 h increased the adhesion number dextran-dose-dependently (Fig. 1B and C).

A proliferation assay was performed to investigate whether dextran affects the proliferation of EPCs. The exposure of 5% and 10% dextran to floating EPCs for 24 h significantly increased the proliferation activity than those not treated with dextran (Fig. 1D).

Dextran increases migration, tube formation, and differentiated EPC colony formation

A migration assay was performed to study whether dextran affects the migration of EPCs. By using a modified Boyden chamber nuclei of migrated cells were observed (Fig. 2A). The exposure of 10% dextran to EPCs for 24 h increased the migrated number (Fig. 2B).

To investigate whether dextran affects the ability of EPCs to form capillary-like tubes, a tube formation assay was examined microscopically (Fig. 2C). A quantitative analysis showed that EPCs exposed to 10% dextran for 24 h increased the sum of the tube structure (Fig. 2D).

We have reported that primitive or definitive types of EPC colonies allow us to predict the potential of EPC differentiation (Masuda et al. 2011). The primitive, small cell sized EPC colony has a higher proliferation potential and is composed of immature EPCs meanwhile the definitive, large cell sized EPC colony has more vasculogenic properties and is composed of differentiating EPCs (Fig. 2E). An EPC colony-forming assay was performed to determine whether dextran affects the endothelial differentiation. The exposure of 10% dextran to EPCs for 24 h decreased the number of primitive EPC colonies, but on the other hand increased that of definitive EPC colonies (Fig. 2F). It indicates that dextran induces endothelial differentiation of circulating EPCs.

Dextran increases the protein and gene expressions of endothelial markers

Floating EPCs were exposed to 5% and 10% dextran for 24 and 48 h, and changes in the surface protein expression rate of the endothelial markers VEGF-R1, VEGF-R2, VE-cadherin, and Tie2, and the activated endothelial markers ICAM1, VCAM1, and integrin αv/β3 were analyzed by flow cytometry. The protein expression level of VCAM1 increased in 24 h-10% dextran EPCs, but others did not change in 24 h-EPCs (Fig. 3A). Every protein level of 48 h-EPCs significantly increased in response to 5% and/or 10% dextran.